Patterns in the Emergent Vegetation of the Rincon Bayou Delta, 2005-2016
Contract #1600011971

Report

by
Kenneth H. Dunton, Ph.D.
Tim Whiteaker, Ph.D.
Michael K. Rasser Ph.D.

Texas Water Development Board

P.O. Box 13231, Capitol Station
Austin, Texas 78711-3231
July 2019

Pursuant to House Bill 1 as approved by the 84th Texas Legislature, this study report was funded for the purpose of studying environmental flow needs for Texas rivers and estuaries as part of the adaptive management phase of the Senate Bill 3 process for environmental flows established by the 80th Texas Legislature. The views and conclusions expressed herein are those of the author(s) and do not necessarily reflect the views of the Texas Water Development Board.

This page is intentionally blank.

This page is intentionally blank.

Texas Water Development Board Report Contract #1600011971

Patterns in the Emergent Vegetation of the Rincon Bayou Delta, 2005-2016

Kenneth H. Dunton
University of Texas Marine Science Institute

Tim Whiteaker
UT Center for Water and the Environment

Michael K. Rasser
Bureau of Ocean Energy and Environment

July 2019

Texas Water Development Board

Table of Contents

List of Figures

List of Tables

Executive Summary

We assessed the percent cover and species composition of the emergent vascular vegetation in the Rincon Bayou Delta (hereafter referred to as the Rincon Delta) to establish a baseline of information for long-term assessment of this unique ecosystem. This work was initiated in part, to evaluate the combined effects of higher salinities from reduced water inflows and sediment delivery to the Delta, relative sea level rise, and increased erosion from wave action on the Rincon Delta. Digital imagery acquired on 15 November 2016 was used to map the current extent of marsh vegetation. The classified imagery was compared to a nearly identical acquisition made on 1 November 2005. Geostatistical analyses using GIS software allowed a change analysis of landscape and vegetation over the 11-yr period. In addition, we were able to make preliminary assessments of the rate of marsh loss on the shoreline of Nueces Bay, which receives constant battering by winds and waves that propagate across Nueces Bay, particularly in spring and summer when southeasterly winds predominate. Our results reveal that the vegetative composition of the Rincon Delta does not appear to have undergone any major system-wide changes over the past decade, despite the inclusion of major drought periods. However, erosion of the Rincon Delta shoreline has continued and perhaps increased, with obvious losses of shoreline and marsh habitat. Some major highlights of our study:

1. Our classification results are the most accurate to date, as reflected by a Kappa Index of 0.70 and overall accuracy of nearly 76%, based on rigorous ground-based collection of data for determination of accuracy assessment (311 sample points) and training data (586 sample polygons) for software imaging calibration.

2. We observed distinct zonation of plant communities in the lower Rincon Delta. The edges of the tidal creeks are dominated by *Borrichia frutescens*, which transition into relatively pure mixed zones of two salt tolerant succulents, *Salicornia virginica* and *Batis maritima*. At increasing distance from the tidal creeks and at still higher elevations, the plant community becomes dominated by *Spartina spartinae*.

3. The most dominant vegetative assemblages are *B. maritima* and *S. virginica* (18%), *Spartina spartinae* (12%), and *Borrichia frutescens* (8%). Water constitutes nearly a third (30%) of the Rincon Delta. These percentages are very similar to that obtained by Rasser (2009) based on the 1 November 2005 imagery.

4. Preliminary estimates show that the erosion of the Rincon Delta shoreline is approximately 4.5 m yr^{-1}. A previous estimate based on an earlier study (Rasser and Dunton 2007) was 2.5 m yr^{-1}. A comparison of 2005 and 2016 imagery illustrates very discernable breaching events of the marsh delta.

5. The increased resolution of the vegetative classification based on intensive ground truthing provides an extremely valuable database for quantifying future changes in vegetation extent and species composition over the Rincon Delta in response to regional climatic change and erosional loss. The detailed documentation of the classification effort and methodology presented here provides a valuable template for future classifications that we recommend on a decadal frequency.

Introduction

Background

The Nueces River Delta (27º 53' N, 97º 32' W) is a tidal marsh system near the City of Corpus Christi, in south Texas (Fig. 1). The Rincon Delta is a component of the larger Nueces Estuary which includes four Bays: Corpus Christi, Nueces, Oso and Redfish (Fig. 1). This system consists of about 5,700 hectares of vegetated wetlands, mudflats, tidal creeks and shallow ponds. The Nueces Bay can be classified as a drowned river valley estuary (Pritchard 1967). However, it also shares characteristics of a barrier estuary (Roy 1984, U.S. Bureau of Reclamation 2000) because of the extensive bar-built bays parallel to the estuary. The climate is semi-arid with a mean precipitation of about 75 cm yr^{-1}. Average tidal amplitude is low with a mean of only 15 cm (Ward 1985). However, occasional irregular tropical storms and hurricanes can provide both large amounts of precipitation and tidal storm surges of several feet (Armstrong 1987).

The Rincon Delta vegetation can be classified as a dry coast type (Adam 1990). Similar dry coast marshes include those of southern California, which share related species, such as the Chenopods (genus *Salicornia*). In contrast, the Rincon Delta is floristically different from the Atlantic Coast marshes, which are often dominated by the grass *Spartina alterniflora*. Despite some similarities in flora, there are significant differences in the physical characteristics of the Nueces Estuary as compared to California estuaries. Many of the estuaries in California were created by tectonic related events such as cracks that formed along fault lines, or when large areas of land sank below sea-level, such as San Francisco Bay. In addition, California has lost most of its wetlands due to human activity. For example, in the San Dieguito Lagoon in San Diego County, 85% of the wetlands were lost between 1928 and 1994 (Kent and Mast 2005).

The Nueces Delta has been significantly modified by humans to provide water to the growing population of Corpus Christi by the construction of two large reservoirs within the Nueces Basin: the Choke Canyon Dam on the Frio River in 1982 and the Wesley Seale Dam in 1958 (U.S. Bureau of Reclamation 2000). Significant research has been conducted since the 1980's examining how reduced freshwater inflow has impacted the Rincon Delta. Early work evaluated the freshwater needs of the estuary in order to develop a water management plan (Henley and Rauschuber 1981). Since then, significant efforts have been conducted to increase freshwater inflow to the Rincon Delta. Perhaps the most significant effort was the Rincon Bayou Demonstration project which constructed an overflow channel (Fig. 2) that lowered the minimum flooding threshold for the upper portion of the Nueces Delta (U.S. Bureau of Reclamation 2000).

Ecological and monitoring studies in the Rincon Delta has largely been funded by a variety of local, state, and federal agencies over the past three decades. A major focus of the past research effort (exclusive of the vegetation mapping effort funded by the Texas Water Development Board based on 2016 imagery) has been the response of plant communities to climatic conditions (Dunton et al. 2001, Forbes and Dunton 2006) and altered freshwater inflow (Alexander and Dunton 2002, 2006). These studies provide evidence that both competition and abiotic factors are important in determining community composition. For example, during drought, the cover of *Salicornia virginica* increased whereas the cover of *Borrichia frutescens* decreased (Forbes and Dunton 2006). Understanding the causes of zonation is important because differences in vegetation patterns can influence important natural processes. For example, an increase in

abundance of shallow-rooted *S. virginica* in favor of the clonal shrub *B. frutescens* may reduce the ability of a marsh to provide shoreline stabilization functions for the coastal community.
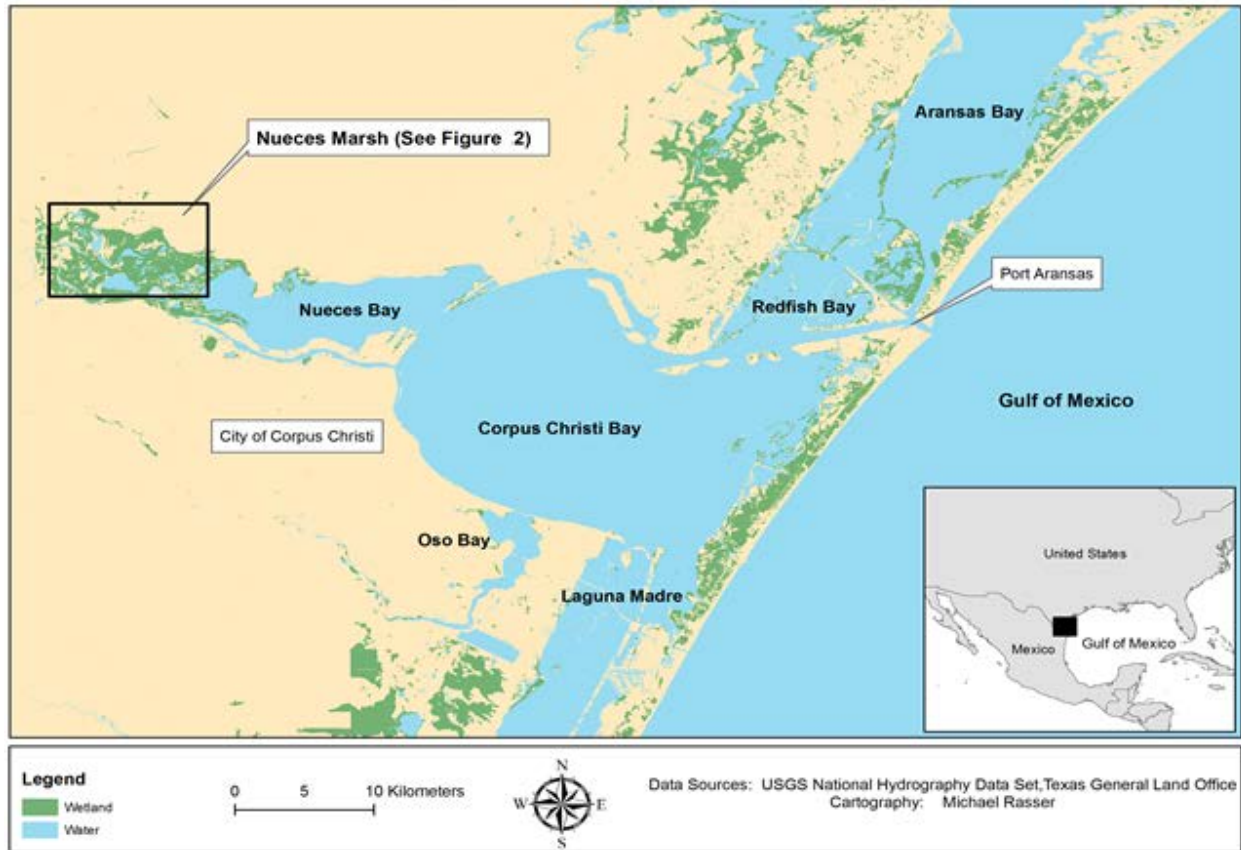
Figure 1. **Location of the Rincon Delta with respect to surrounding bay systems in the Nueces Estuary.**
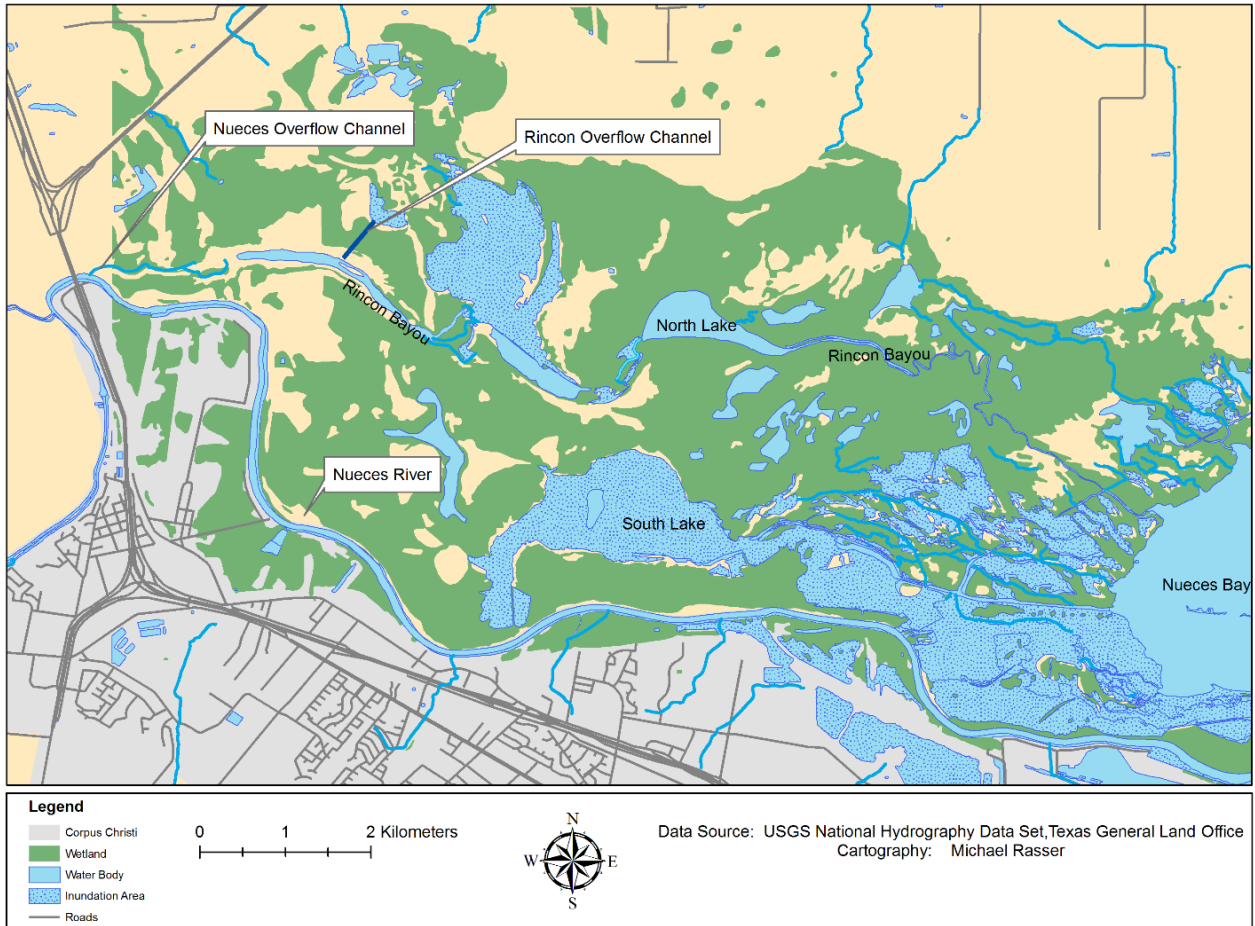
Figure 2. **Key features of the lower Rincon Delta system.**

Project Justification

The Texas Water Development Board (TWDB) executed contracts state-wide to implement adaptive management plans that were developed through the Texas Senate Bill 3 environmental flows process. The University of Texas Marine Science Institute (UTMSI) proposed to examine changes in marsh vegetation in the Rincon Delta over an 11-year period in response to the Rincon Bayou Pipeline freshwater inflows and rapid erosion of the Rincon Delta (Fig. 1). The last acquisition of high resolution, true-color and color infrared imagery (CIR) of the Rincon Delta marsh occurred on November 1, 2005. Support from the Coastal Bend Bays and Estuaries Program allowed acquisition of high-resolution imagery (pixel resolution of one foot) in mid-November 2016 for comparison to the 2005 imagery to ensure an accurate change analysis. Freely available moderate resolution imagery (50 cm resolution from TNRIS, MODIS, LANDSAT, *etc*.) does not provide sufficient resolution to accurately calculate change or to perform precise orthorectification consistent with the 2005 imagery.

Application of Aerial Imagery for Vegetation Mapping

In recent years the use of new digital sensors has proven to be an excellent alternative to film-based aerial photography and satellite sensors. Standard aerial photography is often acquired to map salt marshes because high spatial resolution is useful in determining typical salt marsh zonation. Digital sensors deployed on airplanes have increased in popularity in recent years. These sensors offer several advantages over traditional aerial photography, including a completely digital workflow, improved geometric accuracy and superior radiometric resolution. There is also greater flexibility in the timing of image acquisition than that of standard aerial photography.

Standard aerial imagery can be digitized to create a digital product but the resulting spectral resolution is poor and does not contain discrete spectral bands (Provost et al. 2005). As a result, coastal vegetation mapping utilizing standard aerial photography is most often conducted using onscreen digitizing (for example, see Higinbotham et al. 2004). Multi-spectral digital camera sensors such as the Leica ADS-40 and Z/I DMC (Digital Mapping Camera) offer discrete spectral bands. The digital numbers (DNs) in these images are useful in automated classification methods. In addition, these sensors have high spatial resolution capabilities of up to 0.15 m ground sampling distance, thus offering the ability to examine smaller scale vegetation characteristics such as texture (Chen et al. 2006, Wulder et al. 2004). QuickBird satellite imagery offers a coarser spatial resolution (2.4 m) but similar spectral resolution has been successfully utilized for mapping estuarine wetland plants (Laba et al. 2008).

One method for increasing accuracy of processing remotely sensed imagery is by integrating ancillary data into the original imagery (Wulder et al. 2004). In fact, Lefskey et al. (2002) showed that the integration of other high resolution remotely sensed data such as light detection and ranging (LiDAR) into the original imagery provided a promising avenue for future research. Ehlers et al. (2006) integrated digital surface models and digital mapping camera data to map riparian vegetation in Germany.

According to Wulder et al. (2004), vegetation indices such as the Normalized Difference Vegetation Index (Tucker 1979), Enhanced Vegetation Index (Huete et al. 2002), Soil Adjusted Vegetation Index (Huete 1988) and Modified Soil Adjusted Vegetation Index (Qi et al. 1994) may also be integrated into image processing. All of these indices rely on the relationship between the red and near-infrared bands of the electromagnetic spectrum, and takes into account that plants absorb light in the photosynthetically active range of approximately 0.45 to 0.67µm, and reflect light in the near infrared portion of the spectrum, from 0.7 to 1.3 µm (Lillesand and Kiefer 2004). Selecting a vegetation index for image processing purposes needs to be done carefully because some indices are more effective than others under certain environmental conditions. For example, the normalized difference vegetation index can become saturated when leaf area is very high (Chen et al. 2001). We chose to use a version of the modified soil vegetation index (from Qi et al. 1994) for this analysis because it has been shown to be relatively robust under conditions of low vegetative cover that is typical of the Nueces River delta, and has been proven effective in salt marshes (Eastwood et al. 1997).

The two primary challenges associated with mapping vegetation in the Rincon Delta are (1) vegetation occurs in discrete patches that can vary greatly in size; and (2) the patches of vegetation are often small (sometimes only a few square meters in size). These challenges

require the use of remotely sensed data that has a high spatial resolution (Silvestri 2003) to distinguish between vegetation types. The use of digital color infrared photography has increased in environmental monitoring applications in estuarine systems. Some recent applications include estimation of chlorophyll on exposed mudflats (Murphy et al. 2004), and mapping seagrasses (Lathrop et al. 2006) and aquatic macrophytes (Valta-Hulkkonen et al. 2009).

Salt marshes occur in distinct zones that are the product of physical gradients in stress and competition (Pennings and Bertness 2001). Tidal creeks are important components of coastal salt marshes and determine how much water flow reaches different portions of the landscape (Chapman 1940). The distribution and characteristics of vegetation along tidal creeks also reflect the influences of abiotic and biotic conditions such as salinity and competition. For example, tidal channels influenced the distribution and composition of salt marsh plants in a San Francisco Bay Salt Marsh (Sanderson et al. 2000). However, there is a dearth of studies that have examined the relationship between vegetation and tidal creeks in any salt marsh in the Gulf of Mexico.

The major objective of this study was to characterize the extent and distribution of the major plant assemblages in the Rincon Delta. To accomplish this objective, we used a combination of remote sensing and geospatial analysis. This project quantified the loss of deltaic marsh over time in response to increases in open water areas. It has been well documented that the outer edges of the Rincon Delta are eroding rapidly, at a rate of about 2.5 m yr^{-1} (Rasser and Dunton, 2007). These data provide information that contribute to a broader understanding of the potential roles of decreased freshwater inflows, sediment loading, subsidence, and erosion. The image acquisition occurred in November 2016, nearly exactly eleven years after the last acquisition and the subsequent vegetation classification completed by Rasser (2009).

The classification method employs color infrared imagery from a digital mapping camera (Z/I Intergraph DMC). We used ancillary data such as texture measures, vegetation indices and a high-resolution digital elevation model to increase the information content of the imagery. We also repeated extensive ground surveys to provide both image training data and to assess the accuracy of the mapping methods.

Methods

Ground Data Sampling

As with most salt marsh communities, access and travel throughout the study site is impeded by low bridges, tidal flats, a complex tidal creek network, and very shallow water. In 2005 and 2016, we used a random clustered sampling approach to select ground control points (McCoy, 2005). Thirty-two random points were distributed throughout the study area and within 200 meters of each of these, 16 random points were generated, producing 512 sampling locations. We added another 130 stations for the current study for a total of 642 stations. At each sample point, we visually assessed vegetative cover with a 0.25 m^2 quadrat. In addition, digital photographs and field notes were taken to document ground conditions in the vicinity of each point. In addition, our research group continued to re-occupy transects that were used in the Bureau of Reclamation (BoR) Demonstration Project. We have voluntarily monitored several

transect sites (254, 270, 271, 450, 451, 463) since their establishment in 1999 and thereafter. Results from three sites are reported by Stachelek et al. (2013).

Image Acquisition

We contracted Quantum Spatial, Inc., to acquire the 2016 imagery following the procedures utilized in 2005. The completed data set consists of CIR ortho-corrected digital aerial imagery taken with a large format Z/I Digital Mapping Camera (DMC) delivered in 12-bit uncompressed GeoTIFF format consisting of 62 individual ortho images taken at a pixel resolution of approximately one foot (0.3 meters) ground sample distance in UTM Zone 14 North. Quantum Spatial also provided 16-bit images derived from the 12-bit versions for use with software that cannot handle 12-bit imagery. Four flight lines provided stereoscopic (60% forward overlap, 30% sidelap) coverage of the salt marsh project site at a flight attitude of 10,000 feet-above mean terrain. Airborne GPS and Inertial Measurement Unit (IMU) data were collected during the aerial mission for the orthorectification process. The multi-spectral imagery frames were post processed to produce panchromatic, true color (R, G, B), and false CIR images. Orthorectification to remove radial and relief displacement were performed using camera calibration, Airborne GPS/IMU and a floating point 1-meter DEM derived from LiDAR taken in 2007 (provided by James Gibeaut and Anthony Reisinger at the HRI, TAMU-CC). A nearest neighbor resampling algorithm was employed during the rectification process to create the CIR ortho images that had a resolution of one-foot ground sample distance. CIR ortho images were delivered in TIFF format with associated TFW header files based on UTM Zone 14 North (meters) Coordinate System (NAD 1983 datum). No radiometric balancing was applied, no mosaicking of individual image frames was performed and no post rectification editing (using Photoshop) to manipulate any pixels for aesthetic purposes was conducted in order to preserve the spectral signatures of the original CIR images.

A classification of the imagery was conducted using an analysis of the newly acquired data and other ancillary data following the sequence described below:

1. Creating the Mosaic

    Images of the study area were combined to create a single mosaic. The resulting image was clipped using a shape file of the study area.

2. Use of Ancillary Data

    An accepted way of increasing the accuracy of processing remotely sensed imagery is through the integration of ancillary data (Wulder et al., 2004). We used a modified soil vegetation index (MSAVI, Qi et al., 1994), a measure of vegetation texture (Rasser, 2009), distance from water, and LiDAR data as ancillary layers in the mosaicked imagery.

3. Classification

    Classification was conducted using the four-band digital image, along with ancillary data. The classification was used to build several vegetation classes based on ground-truth data and photo interpretation.

The 2016 Study Area

PIs Dunton, Whiteaker and Rasser worked together to identify the target area for mosaicking and analysis. Starting with the 2005 area, they added two new sampling areas in the northeast (1 cluster) and southern (2 clusters) zones. Using the acquired imagery, a 1-meter DEM, and publicly available contextual layers such as land cover[1], soils[2], and the ecological mapping system of Texas[3], areas that were clearly uplands and not pertinent to this study were excluded. The resulting area as shown by the thick outline forms the boundary of subsequent analyses performed for this project (Fig. 3).

Creating the Mosaic

We initially planned to perform the analysis in ArcGIS for Desktop 10.5 and ERDAS IMAGINE 2016, the programs and versions for which we had licenses at The University of Texas at Austin. However, IMAGINE lacked more advanced classification algorithms then ArcGIS (such as Support Vector Machine and Random Forest), and its mosaic seamlines were inferior to those produced by ArcGIS in testing. Consequently, we decided to perform the analysis purely in ArcGIS.

We created a mosaic of the analysis area with the objectives of minimizing color corrections between images. Assuming that atmospheric conditions are more likely to be consistent within a given flight line than across flight lines, we selected images from flight lines 2 and 3, leaving out flight lines 1 and 4, which cover the northern and southern boundary of the area. Although there is enough overlap amongst the images to skip every other image without leaving gaps, we included all images within the desired tile range for a given flight line in order to minimize brightness differences across images. Brightness appears to increase in all images from east to west, which results in poor histogram matching between the western portion of one image and the eastern portion of another. By using all images and prioritizing the eastern portion of each image, we removed the western edge from the matching, which improved the overall mosaic without any color corrections applied. The final set of images used includes images O2_09 (i.e., flight-line 02, image 09) to O2_17 and O3_06 to O3_17. We used the 12-bit version of the images provided by Quantum Spatial rather than the derived 16-bit versions that they provided since ArcGIS handles 12-bit images without issue.

---

[1] U.S. Geological Survey (2014). NLCD 2011 Land Cover (2011 Edition, amended 2014) - National Geospatial Data Asset (NGDA) Land Use Land Cover. Downloaded from https://tnris.org/data-catalog/entry/national-land-cover-database-2011/ (accessed 2017-04-20).

[2] USDA Natural Resources Conservation Service (2011). Soil Survey. Downloaded from https://tnris.org/data-catalog/entry/soils/ (accessed 2017-04-20).

[3] TPWD Missouri Resource Assessment Partnership (MoRAP) and Texas Natural Resource Information System (TNRIS) (2009). Western Gulf Coastal Plain; Ecological Mapping Systems of Texas: 398 Mapped Types. Downloaded from https://tnris.org/data-catalog/entry/tpwd-texas-ecological-systems-data/ (accessed 2017-04-20).
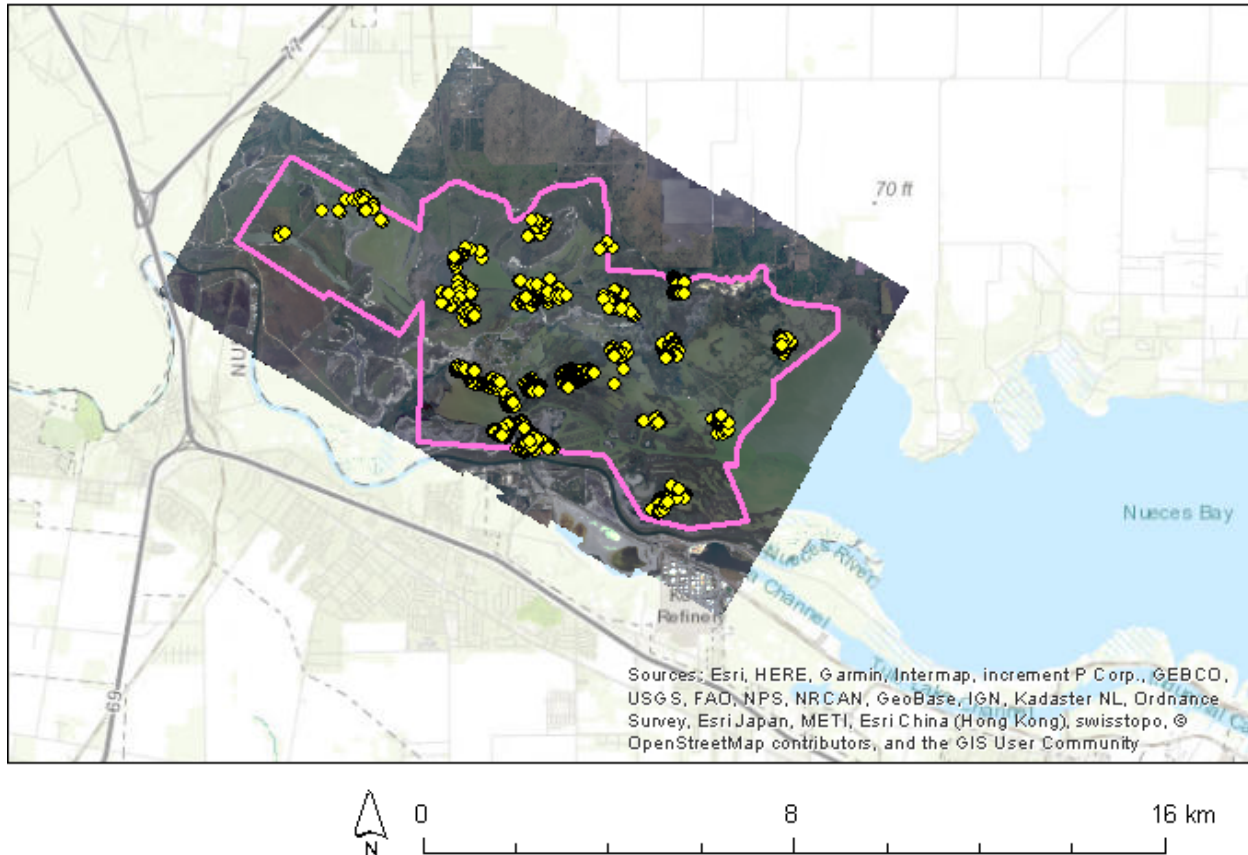
Figure 3. **Project study area (pink boundary) containing stations visited (yellow dots), with imagery dataset as a backdrop.**

To prepare the images and create the mosaic in ArcGIS for Desktop:

1. Set 0 as NoData for all bands using the **Set Raster Properties** tool.

2. Build pyramids and calculate statistics for each raster using the **Build Pyramids and Statistics** tool.

3. Create the mosaic in a geodatabase by right-clicking a geodatabase in the Catalog window and clicking **New > Mosaic Dataset**, and then setting these properties.

   a. Coordinate System: NAD_1983_UTM_Zone_14N

   b. Product Definition: None

   c. Number of Bands: 4

   d. Pixel Type: 16_BIT_UNSIGNED

4. Right-click the mosaic dataset and click **Add Rasters** to add images from the workspace (i.e., folder) containing the image files, using all defaults.

5. Right-click the mosaic dataset and click **Enhance > Generate Seamlines**. The software determines the optimal seamlines defining which image is displayed where adjacent images overlap.

6. Right-click the mosaic dataset and click **Enhance > Calculate Statistics**. This computes statistics for the whole mosaic, enabling symbology adjustments.

7. Right-click the mosaic dataset and click **Optimize > Build Overviews**. These enables faster display at small map scales.

8. Add the mosaic to ArcMap to verify that images were added and seamlines were generated.

9. Right-click the **Image** layer with the mosaic in the ArcMap Table of Contents and click **Export Data**. Set **0** as the NoData value, set **TIFF** as the format with no compression and click **Save**. Saving as a TIFF merges all images into a single image and enables the mosaic to be viewed in other geospatial software if this dataset were to be used in future work.

10. Use the **Clip** geoprocessing tool to clip the exported mosaic to the study area, saving the result as **ImageMosaic.tiff**.

Color Balancing

Color matching across seamlines, the borders between the portions of adjacent images actually used in the mosaic, was generally very good in the raw mosaic without any color corrections (Figure 4). We evaluated color matching options in both ArcGIS and IMAGINE, and found no result exhibited substantially improved blending across seamlines, and so no color balancing was applied to the mosaic.
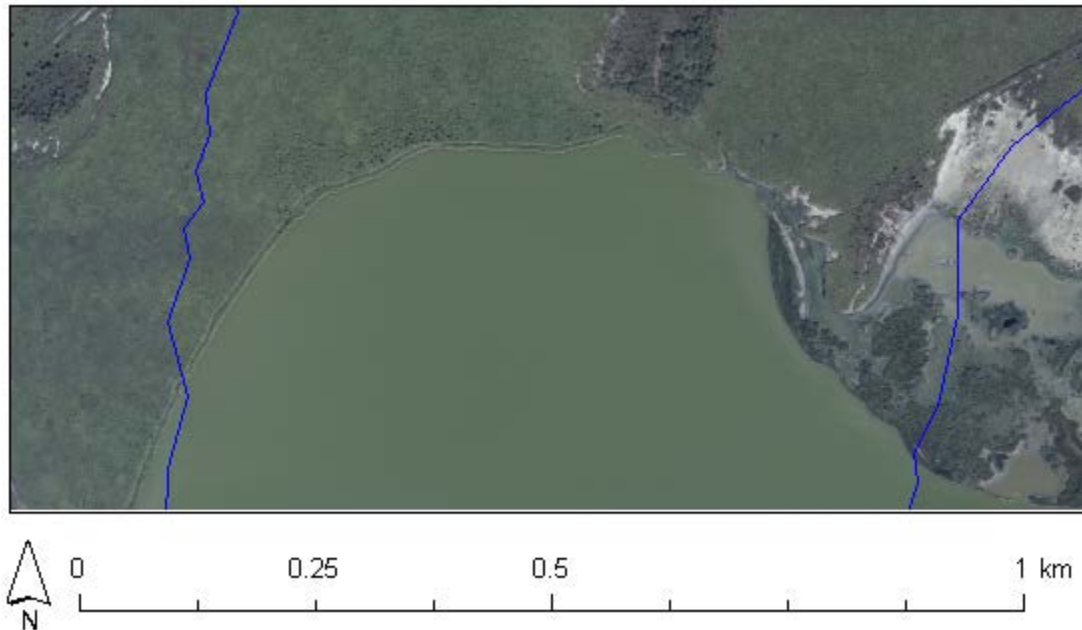
Figure 4.   **Matching across seamlines (blue lines in the figure) is generally very good in the raw mosaic.**

Field Work

Visits to the marsh provide valuable geotagged photographs and percent cover evaluations. This information was used as training data and accuracy assessment data, where training data is used to train the image classifier and accuracy assessment data is used to evaluate accuracy of the resulting classification. The following abbreviations were used for ground cover categories in training and accuracy assessment data:

- *BF*   *Borrichia frutescens*
- *BM*   *Batis maritima*
- *DS*   *Distichlis spicata*
- *LC*   *Lycium carolinianum*
- *LN*   *Limonium nashii*
- *ML*   *Monanthochloe littoralis*
- *SA*   *Spartina alterniflora*
- *SB*   *Salicornia bigelovii*
- *SL*   *Suaeda linearis*
- *SS*   *Spartina spartinae*
- *SV*   *Salicornia virginica*
- O   Other

Accuracy Assessment

We targeted accuracy assessment points based on the approach used by Rasser (2009). Not all points could be visited due to difficulty in accessing some sites, and some points were excluded from accuracy assessment because they either fell outside of the study area (which was defined after some of the earlier field visits) or because their locational accuracy seemed questionable when plotted on the imagery. The preliminary accuracy assessment point set included 642 points, of which 311 were used in the final accuracy assessment.

For each assessment location, the following procedure was followed:

1. Using the Trimble GPS, visit the precise point using the waypoints from the 2005 GPS Data.

2. Collect percent cover data.

3. Take photos in all four cardinal directions (N-E-S-W) and one photo of the quadrant itself. We used a camera that provided a bearing or displayed a bearing in the photo (e.g., colored duct tape on quadrat).

4. Photograph field notes so that they are also georeferenced.

Note that the data did not include significant cover of DS, LN, LC, SB, SA, and SL, making accuracy assessment difficult or impossible for these species. Therefore, these categories are

combined into Other for the purpose of accuracy assessment. A dominant category is assigned to each point if that category comprises more than 50% of the cover for that location.

Training Data

We collected over 1,200 random photos made with the Garmin GPS camera and selected examples of pure stands of the major marsh plant species, deep water, and bare substrate types. Representative photos were added to the training data set. We divided non-vegetated substrate into wet, damp, and dry blue green algal cover categories to test for spectral differences (Fig. 5, 6).
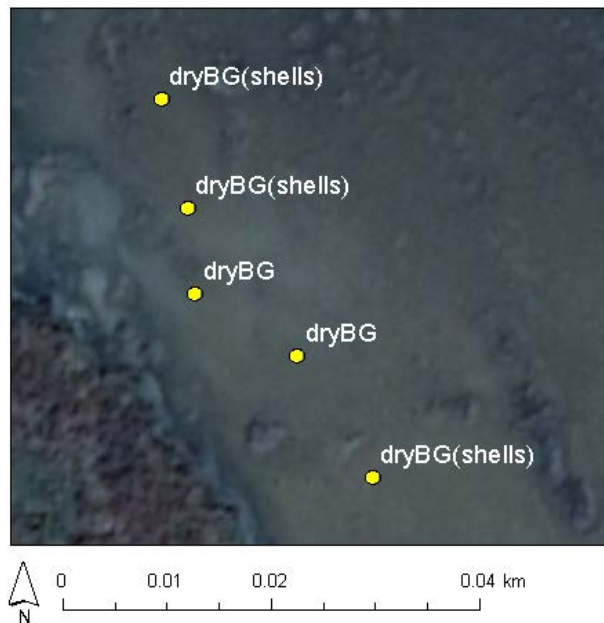
Figure 5.   **The bivalve middens with hundreds of white shells on a blue green algal substrate appeared spectrally the same as the dry blue green areas without the shells. This result was unexpected but instructed us to combine these categories.**
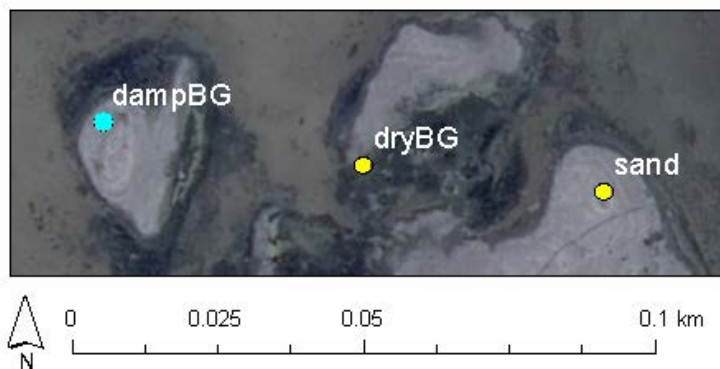
Figure 6.   **It is apparent that the substrate subcategories (dry, wet, damp, with shells) assigned from the photographs were not useful. Blue green algae population appearances can change very quickly with water input which creates a spectral color shift.**

All marsh substrates are composed of mud with varying fractions of sand and blue green algae. The blue green algae appear across the color spectrum from almost black (thick and wet) to white (dry, salty) and all shades in between. It can also change appearance quickly with the addition of water from overflow or rain which makes ground-truthing post acquisition unreliable. Therefore, we combined these subcategories into one non-vascular plant vegetated substrate.

Ground truth surveys began on 14 November 2016 and were completed 14 March 2017 (Table 1). Over 70% of the random locations were visited over a six-week period in January and February 2017. This winter period is marked by considerably cooler temperatures that essentially preserve the foliage at its late autumn peak condition, since the plants are in a physiologically dormant state. All photos were made with a Garmin GPS camera (Model 645C) and georeferenced with an associated latitude and longitude. The high-resolution photographs can be displayed at their exact location in any mapping application. We believe that these photographs greatly enhanced our ability to check the classifications made from the aerial images.

Table 1. **Ground truthing observations at 311 random locations for accuracy assessment occurred over a 3-month period, from 14 November 2016 to 14 March 2017.**

	Random Point Type				
# Field Days	Random Points for Accuracy Assessment	Water	Unvegetated	Vegetated (includes ALL species in final classification)	Other Remaining Vegetation
12	311	106	56	99	50

In addition to visiting 311 random locations to calculate metrics for accuracy assessment, we also occupied specific locations that were dominated by specific cover types to "train" the software to recognize those specific signatures as specific vegetation or substrate types. The 586 non-random points were derived from several sources:

1. Geotagged photos from visits to the marsh from which dominant cover types were subsequently identified
2. Guidance from Kim Jackson, an expert on the marsh area, in a two-day session of evaluating imagery onscreen in locations where Ms. Jackson had confident knowledge on ground cover types. These included, for example, identification of forested areas or railroad tracks, or areas that are perennially covered with water.
3. Transects from another study conducted by Ms. Jackson with a field visit in December 2016, just one month after the imagery was flown. These transects provided 199 points around six sites for which percent cover data was recorded.
4. Amongst accuracy assessment points with questionable locations, some were relocated based on photos and imagery when the correct location was clear. However, because we

modified the point, we chose not to use it for accuracy assessment but rather for training data.

Using these resources, Dr. Whiteaker drew polygons over the imagery, thereby defining pixel locations to be used as training samples for the classification (Fig. 7). These polygons are created interactively using the Image Classification toolbar in ArcMap. The final training shapefile was saved as TrainingSamples.shp. The samples included the following categories and numerical codes:

- BF - 2
- BM - 4
- BM_SV (combined class) - 4001
- SS - 10
- SV - 12
- forest - 21
- rrtrack (railroad track) - 23
- sand - 24
- bare - 8000
- other (other vegetation) - 9999
- water – 51
-
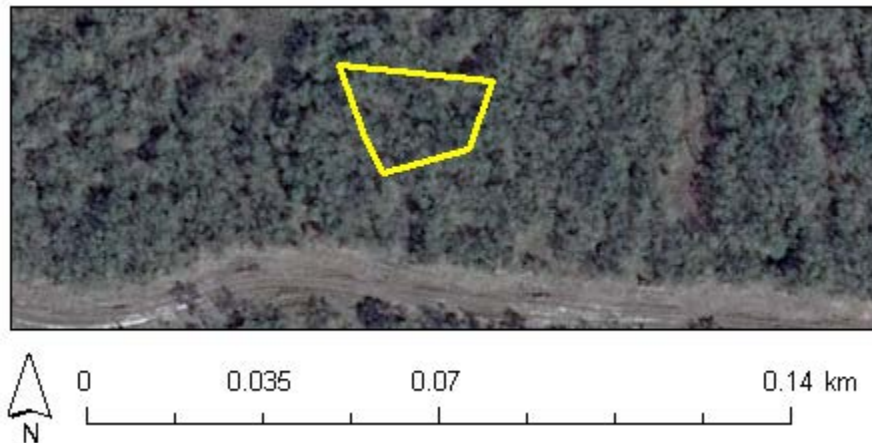
Figure 7.   **Example training sample polygon for the forest category.**

Categories such as forest and sand are retained to facilitate comparison with Rasser (2009), even though they are not explicitly represented in the accuracy assessment categories. Since accuracy for these categories cannot be assessed systematically, caution should be used when evaluating a classified raster based on the full set of training sample categories.

Use of Ancillary Data

Rasser (2009) appended the following bands to the imagery in order to provide additional information for the classifier to utilize:

- Elevation
- MSAVI (Modified Soil-Adjusted Vegetation Index)
- Texture (standard deviation of MSAVI)

For this project, we included those bands plus a band representing distance from tidal creeks and other significant water bodies. Some classification algorithms work best when the various analysis bands have roughly the same range of pixel values. Therefore, the general procedure is to align all bands to the same grid, resample to the same cell size, convert to the same numerical type (e.g., integer), and scale values to match the range of pixels in the imagery. For example, if imagery values ranged from 0 to 100, and elevation values ranged from 0 to 25, one could multiply elevation values by four to scale them to 0 to 100.

Elevation

This project utilizes a floating point 1-meter DEM derived from LiDAR taken in 2007 (provided by James Gibeaut and Anthony Reisinger at the HRI, TAMU-CC). To make the DEM usable for image classification, several issues were addressed:

- The DEM has gaps, presumably where the presence of water limited LiDAR efficacy.
- The DEM does not cover the entire extent of the study area.
- The DEM has a one-meter cell size, whereas the imagery has a 0.3-meter cell size.
- The DEM has a different value range than the imagery.

The gaps and lack of study area coverage are addressed by assigning values to the DEM where it presently has NoData. A technique called Nibble is applied to achieve this. Nibble replaces designated cells with values from the nearest neighbor. Since the DEM has very large gaps, nibble works better than the other commonly used gap filling method of computing a focal mean. With focal mean, the large gaps require a large search radius, which captures pixels far away, which results in water areas being overly elevated due to the influence of nearby uplands.

Once gaps are filled, the DEM is then resampled to use the same cell size as the imagery data and to align it to the imagery grid. The bilinear resampling technique is used since a DEM represents continuous data. While this does result in some smoothing of the data, the motivation for using a DEM is to help the classifier broadly distinguish uplands from lowland areas, and the magnitude of local smoothing of the data should not significantly impact identification of uplands. Note that the DEM is in the same coordinate system as the imagery, so the DEM does not need to be re-projected.

The DEM was processed in ArcGIS for Desktop using geoprocessing tools. The ArcGIS Nibble tool takes as inputs a raster dataset to be nibbled and a mask raster. The input raster must be of integer type, and NoData cells within it are not processed. The mask raster must also be of

integer type. Wherever NoData cells occur in the mask raster, the corresponding cells in the input raster will be replaced with the values of the nearest neighbor.

To process the DEM:

1. Convert the DEM to an integer raster.
    a. Run the **Times** tool to multiply the DEM by 10,000. The preserves some portion of the DEM values to the right of the decimal point.
    b. Convert the result to integer by running the **Int** tool. This truncates values beyond the decimal point, but the accuracy loss is negligible.
2. Fill NoData values with a value of -99999.
    a. Run the **IsNull** tool on the integer DEM to produce a grid with a value of 1 where the input is NoData and 0 otherwise.
    b. Run the **Con** tool, using the result of the previous step as the conditional raster, -99999 as the value if the conditional raster is 1, and the integer DEM for when the conditional raster is 0.
3. Run the **Nibble** tool to replace -99999 with the nearest neighbor from the integer DEM.
    a. Use the result from the previous step as the input raster.
    b. Use the original integer DEM as the mask raster.
    c. Uncheck "Use NoData values if they are the nearest neighbor".
4. Run the **Resample** tool on the DEM to match the grid used for the imagery.
    a. Use the nibbled DEM as the input raster.
    b. Use a cell size of 0.3.
    c. Use the bilinear resampling technique since a DEM represents continuous data. We use bilinear instead of cubic convolution to reduce the impact of smoothing on the data.
    d. In the Environments window, set the imagery mosaic raster as the snap raster.
5. Run the **Clip** tool to clip the result of the previous step to the study area.
6. The clipped DEM ranges in value from -41200 to 215604 (it's the relative rather than absolute difference between values that is important at this point), whereas the highest value in the imagery is 3839 in band 4. To rescale the DEM, add 41200 using the **Plus** tool and then run the **Divide** tool to divide the resulting values by 67. The highest value in the result is 3832 and the lowest is zero.
7. Export the result as Elevation.tif if a standalone copy is desired (Figure 8).
8. Use the **Composite Bands** tool to append the elevation band to the imagery mosaic.

Modified Soil Adjusted Vegetation Index (MSAVI)

The Modified Soil Adjusted Vegetation Index (MSAVI; Qi et al. 1994, Fig. 9) is derived from Red and Near-Infrared imagery bands. MSAVI was calculated in ArcGIS using the predefined **Band Arithmetic** function.

The MSAVI raster was rescaled using the **Times** tool to multiply values by 2000, then converted to integer using the **Int** tool before adding it to the composite raster using the **Composite Bands** tool.
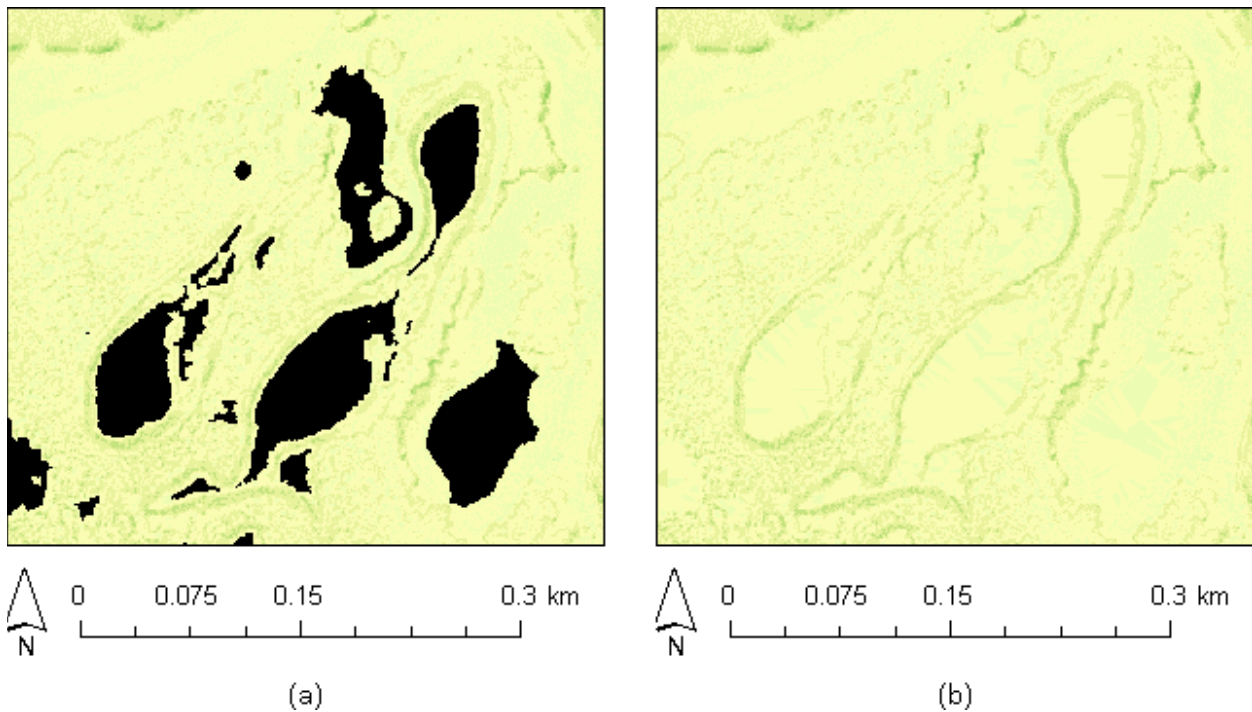
Figure 8.   **DEM areas (a) with gaps shown in black, and (b) with gaps filled.**
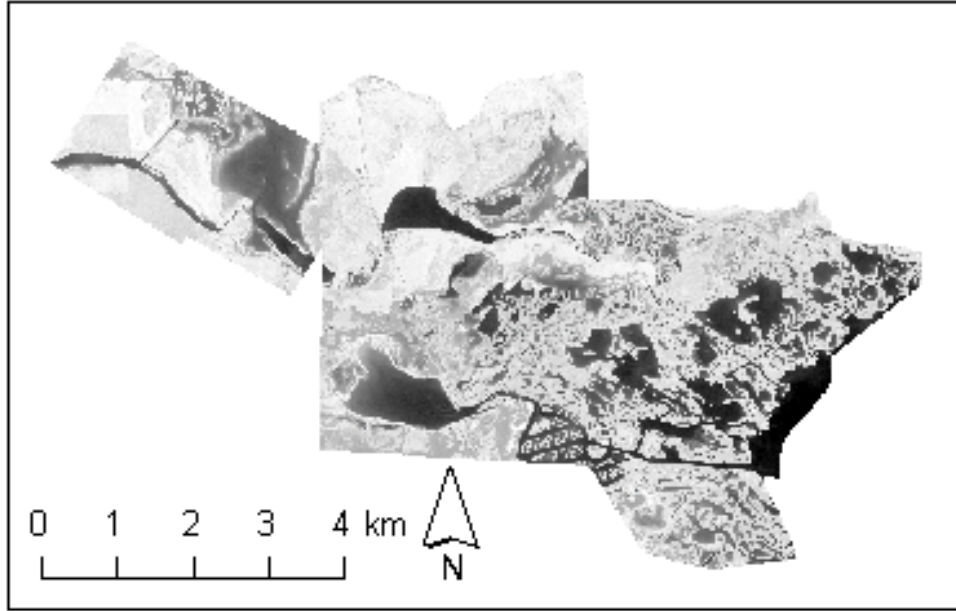
Figure 9. **The data layer created in Modified Soil-Adjusted Vegetation Index, MSAVI.**

Texture

Texture is derived from MSAVI via a 3-by-3 moving window from which MSAVI standard deviation is calculated using the Raster Function Properties in ArcGIS.

The resulting raster was rescaled using the **Times** tool to multiply values by 10000, then converted to integer using the **Int** tool before adding it to the composite raster using the **Composite Bands** tool (Fig. 10).
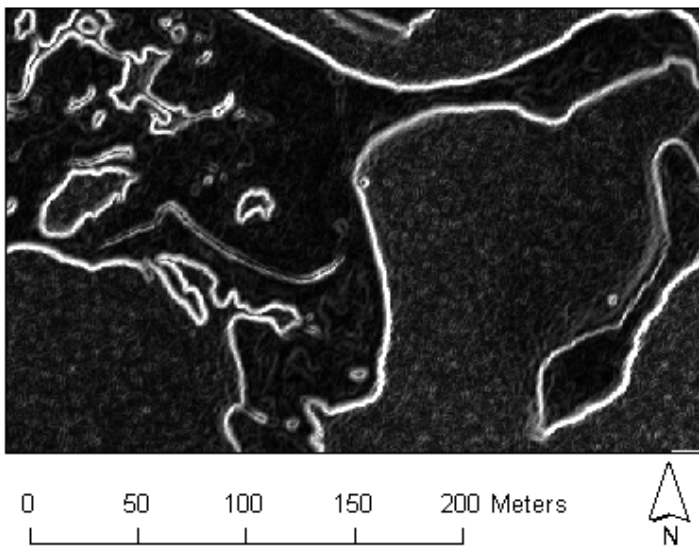
Figure 10. **Example of texture in an area along the bay.**

Distance from Water

Using the composite raster which includes imagery, elevation, MSAVI, and texture bands, a random forest classification was run with an earlier version of training samples to produce a classified raster that included water as a category. (That version of training sample data included SA and AG samples created with guidance from Jackson, which were later removed from the final analysis. The delineated water areas were deemed sufficient to use for estimating distance from water without repeating the analysis with the final training dataset.) The procedure for performing the classification is described in more detail later in this document.

With a raster including water pixels in hand, the procedure to compute distance from water is:

1. Use the **Set Null** tool to set non-water pixels (Classvalue <> 51) to NoData.
2. Use the **Region Group** tool to identify contiguous regions of water.
3. Use **Raster to Polygon** to convert the region raster to vector features.
4. Select tidal creeks and bodies of water that are known to be perennially inundated (local knowledge from Kim Jackson).
5. Use **Polygon to Raster** to convert the selected polygons back to raster. The original imagery was used as the snap raster and to provide the extent, while the study area boundary provided a mask, so that the result conforms to the raster used for classification.
6. Use the **Euclidean Distance** tool on the result of the previous step to compute distance from water.
7. Use **Times** to multiply the result by 2 in order to rescale the raster so that values are comparable to those from the imagery.
8. Use **Int** to convert the result to integer.
9. Use Composite Bands to add the result to the existing composite raster containing all other bands to be used for image classification (Fig. 11).
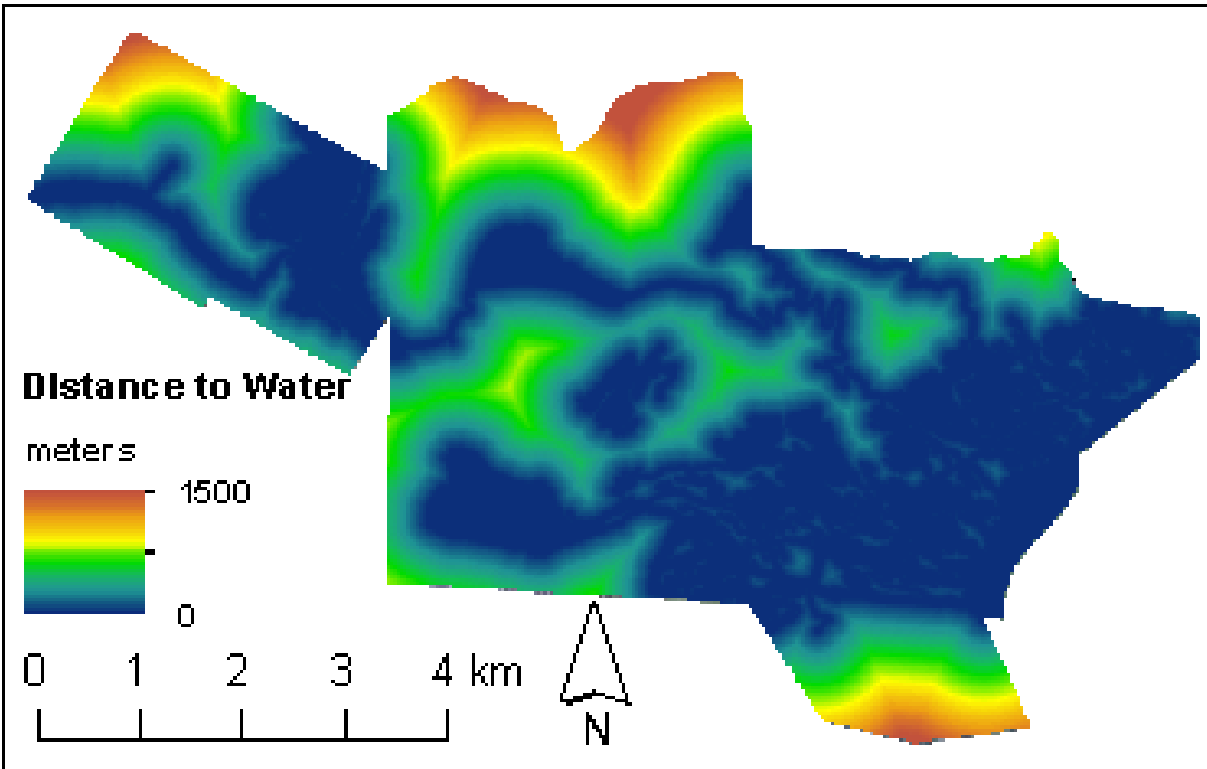
Figure 11. **The distance to water GIS layer.**

Classification

Several ArcGIS classification tools were tested along with several combinations of ground cover categories. In general, we found that Random Trees (the ArcGIS name for Random Forest) performed the best, and that combining classes that are hard to distinguish in the imagery such as BM and SV improved results. Some classes in the training data such as rrtrack (railroad track) were easy to distinguish and so were retained in the classification; however, since rrtrack does not exist as an accuracy assessment category, it is merged into bare before accuracy is assessed.

The procedure to produce a classified raster is:

1. Run the **Train Random Trees Classifier** tool with these inputs:
   a. Input Raster - CompositeRaster
   b. Input Training Sample File - TrainingSamples.shp
   c. Output Classifier Definition File - RT.ecd
   d. Max Number of Trees - 128
   e. Max Tree Depth – 70

2. Run the **Classify Raster** tool using the composite raster and the classifier definition file as inputs. The resulting raster includes all classes in the training data, some of which

were used in Rasser (2009) but are not in the current accuracy assessment set of categories.

3. Run the **Reclassify** tool to reclassify class values as follows:
   a. 4 (BM) and 12 (SV) to 4001 (BM_SV)
   b. 21 (forest) to 9999 (other)
   c. 23 (rrtrack) and 24 (sand) to 8000 (bare)
   d. Retain the remaining classes as their original class value (Fig. 12).
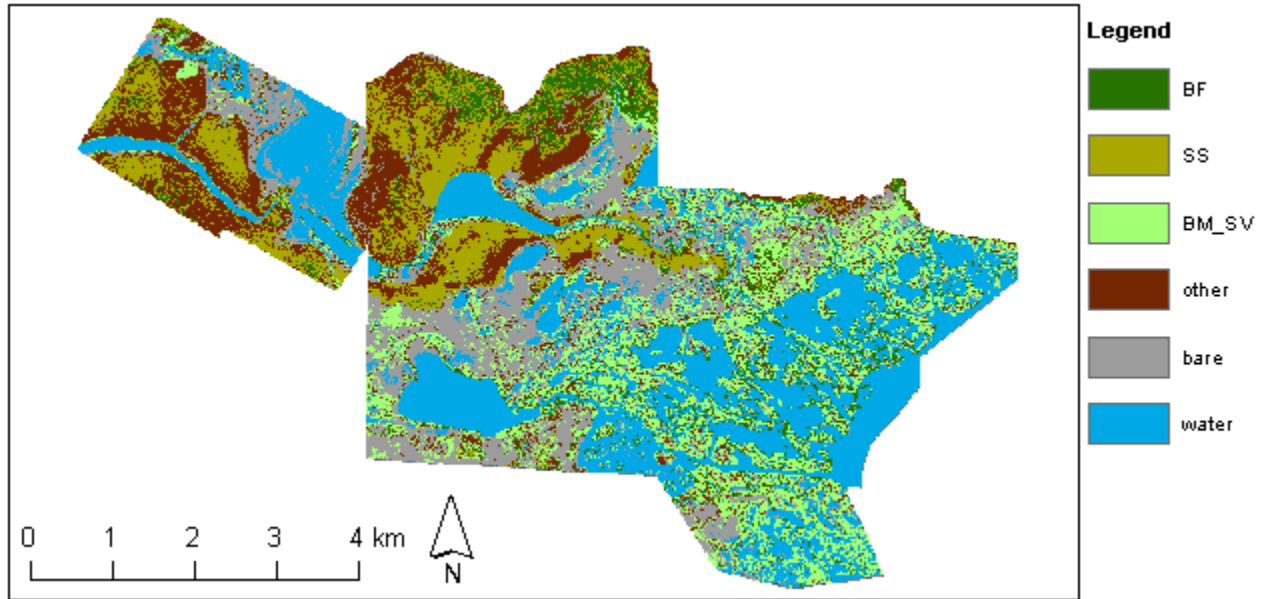
Figure 12.   Final classes in the reclassified result.

Assessing Results

1. Import accuracy assessment points into GIS.
2. Remap the assessment categories into the following categories which reflect what the we think can be reasonably interpreted from the input data:
   a. BF remains BF
   b. BM and SV to BM_SV
   c. DS, LC, LN, ML, SA, SB, and SL to other
   d. SS remains SS
   e. O remains Other
   f. Water remains Water
   g. Bare remains Bare
3. Add Long Integer fields named Classified and GrndTruth to the point features. These fields are used by ArcGIS when assessing results.

4. Assign -1 to the Classified field and assigned the class number associated with each class from the Training Sample Manager to the GrndTruth field, e.g., a value of 2 for BF points and 51 for water points.

5. Run the **Update Accuracy Assessment Points** tool, using CLASSIFIED as the target field. This assigns the class number from the raster to the Classified field in a new feature class.

6. Run the **Compute Confusion Matrix** tool using the updated assessment points from the previous step (Table 2).

The key for the confusion matrix class values is:

- 2 = BF
- 10 = SS
- 4001 = BM_SV
- 51 = Water
- 8000 = Bare
- 9999 = Other

Table 2.   The Confusion Matrix for the 2016 classification analysis. n/a = not applicable

ClassValue	C_2	C_10	C_51	C_4001	C_8000	C_9999	Total	U_Accuracy	Kappa
C_2	10	1	0	4	0	5	20	0.5	n/a
C_10	2	26	0	0	0	3	31	0.83871	n/a
C_51	1	0	95	0	0	1	97	0.979381	n/a
C_4001	0	0	4	42	11	13	70	0.6	n/a
C_8000	1	0	6	3	39	4	53	0.735849	n/a
C_9999	1	4	1	4	6	24	40	0.6	n/a
Total	15	31	106	53	56	50	311	0	n/a
P_Accuracy	0.666667	0.83871	0.896226	0.792453	0.696429	0.48	0	0.758842	n/a
Kappa	n/a	n/a	n/a	n/a	n/a	n/a	n/a	n/a	0.695098
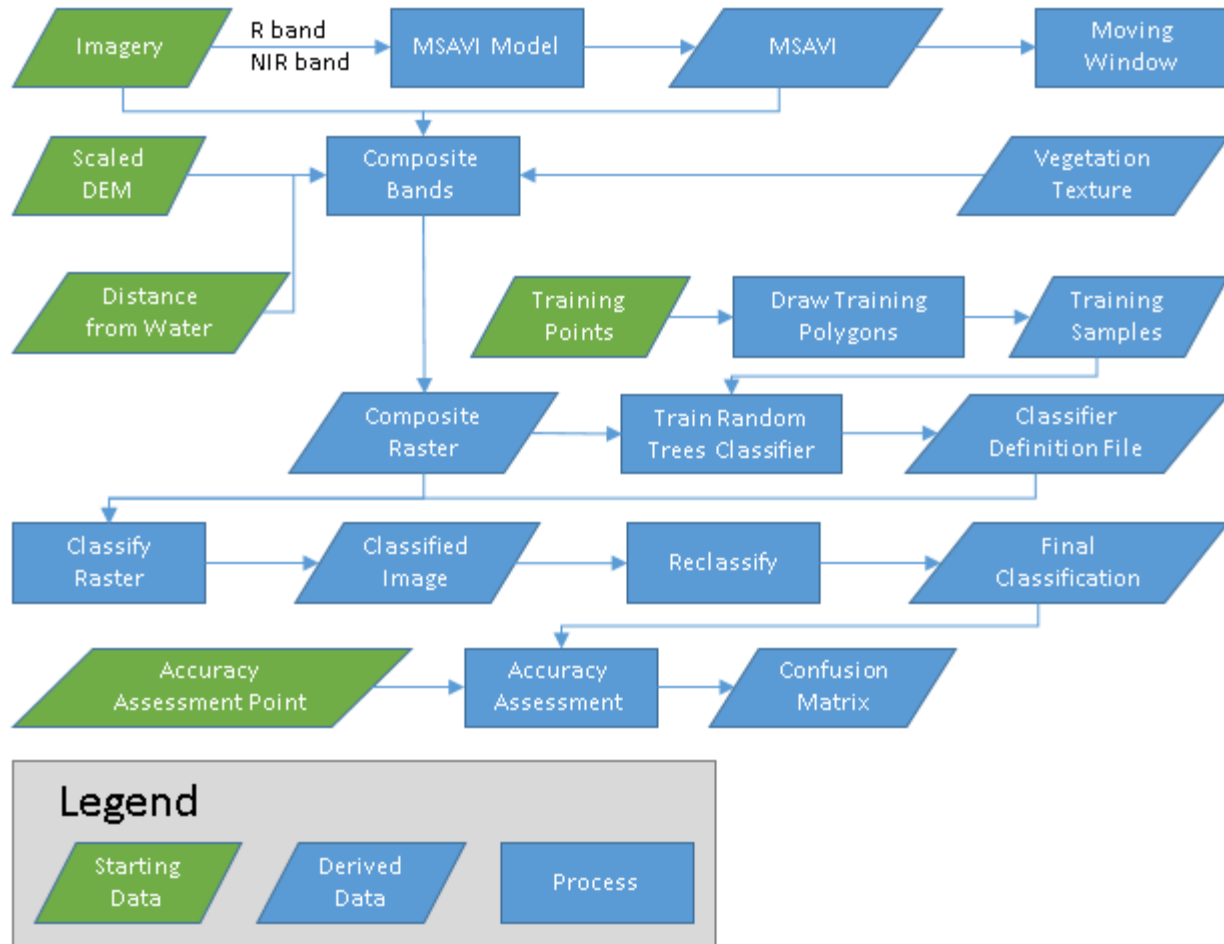
Figure 13. **The Image Classification Flowchart. Note the incorporation of Ancillary Data layers as described above.**

Change Analysis, 2005-2016

GIS data layers were created to compare the results of the 2005 and 2016 vegetation patterns. Study areas from 2005 and 2016 were intersected, and this common study area was used to clip 2005 and 2016 classified results. We used this process to examine changes in losses and gains in vegetation (overall and by assemblages). The image acquisition on 1 November 2005 and 15 November 2016 occurred during periods of very similar water elevation levels based on tidal records, precipitation events, and analysis of the acquired imagery. The image acquisition in the morning of both days occurring during periods of slack low water (-0.25 to 0 feet above MSL) following an ebb tide and preceding a flood tide (https://tidesandcurrents.noaa.gov/map/index.html?id=8775237). There were also no major precipitation events that preceded the acquisition on either date that would have produced flooding events in the Delta. For the 30-day period preceding acquisition in 2005, rain accumulation was 3.15 inches spread almost equally among three events, compared to 2016, which had a total rainfall of 1.06 inches that mostly fell in one rain event

(https://www.climate.gov/maps-data/dataset/daily-temperature-and-precipitation-reports-data-tables). Finally, analysis of the imagery revealed no overbanking during the period of acquisition, nor any evidence of extremely low water levels based on the appearance of water filled tidal creeks that appeared identical in appearance between 2005 and 2016 imagery. Dates in November were carefully selected based on overall climatic and tidal stability. The acquisition was supplemented by the monitoring of vegetation changes along three transects established in 1999 and 2000 (stations 254, 270, 450), which were also assessed and reported as part of this project.

Vegetation and Porewater monitoring

The abundance and distribution of emergent plants was monitored quarterly for one year starting fall 2017 at three sites in the lower marsh. The resulting dataset documents observed changes in seasonal plant community composition and coverage since monitoring began in 1997. The abundance of emergent plants for this time period was estimated from percent cover data collected within 0.25 m^2 quadrats (percent cover data was used as a proxy for abundance). Measurements were taken at 2-m intervals along 6 parallel 10 m transects (30 quadrats / site) at each of three sites. Soil characteristics were obtained by extracting water from soil cores (2.5 cm diameter x 10 cm length) by centrifugation. The extracted water was analyzed for salinity using a handheld refractometer (Reichert Scientific Instruments, Buffalo, NY). Quarterly sampling (percent cover and plant composition was completed at sites 254, 270, and 450 on the following dates: 27 November 2017, and 19 March, 29 June, 28 September and 18 December 2018.

Data Archival

We propose to archive datasets from this work with the Texas Natural Resources Information System (TNRIS). We have contacted TNRIS, and they confirmed that they are willing and able to house our data should we choose to archive with them. We plan to archive the following datasets:

- Original images from 2016 (62, in 12-bit format)
- Mosaicked image (21 images from 2016, unclipped)
- 2016 study area shapefile
- Raw classified result, which includes 11 classes
- Reclassified result for accuracy assessment, 6 classes
- Accuracy assessment points
- Confusion matrix

A confusion matrix was created using 311 points, none of which had been used in the training process (Table 1). The mapped class of each point was determined by comparing the mapped value in the classified image with the previously determined reference class based on the ground data. The reference class was chosen by selecting the class that contained most of the percent cover based on field sampling. For example, if a site contained 80% water and 10% sediment it was classified as water. The user and producer accuracy and the overall accuracy and Kappa Index were calculated for each class (Table 3). We will include a description for the GIS procedure used to create the classified result, similar to the methodology section, and metadata associated with the imagery provided by Quantum Spatial, Inc.

Results and Discussion

Vegetation Classification

The results of this study demonstrated that salt marsh plant communities can be accurately mapped utilizing supervised classification of imagery integrated with ancillary data. We obtained a Kappa Index of 0.70 and overall accuracy of nearly 76% (Tables 2 and 3) compared to the medium level of matching (Landis and Koch 1997 that Rasser (2009) obtained in the 2005 classification (Kappa Index 0.41 and overall accuracy 57%). Our results are likely a product of the large numbers of points we used for training the software and samples used for accuracy assessment. Sadro et al. (2007) had an average overall accuracy of 59% with a Kappa coefficient of 0.40 for a supervised classification of plant distribution in California, which consisted of six classes. In another study, Gilmore et al. (2008) had a high accuracy utilizing multi-temporal satellite imagery combined with LiDAR vegetation canopy data to map wetland vegetation in tidal wetlands of the lower Connecticut River. This higher accuracy was attributed to their using a multi-temporal data set consisting of QuickBird multi-spectral imagery, which allowed for differentiation of species based on phenology.

In the past few years there has been substantial research on integrating LiDAR data with hyperspectral data such as CASI (Verrelst et al. 2009). Classification appears to be somewhat more accurate as compared to the multi-spectral imagery incorporated in this study. For example, Pengra et al. (2007) had higher accuracy (overall accuracy = 81.4%) in mapping marsh plants on the west coast of Greenbay, Wisconsin using hyperspectral imagery as opposed to using multi-spectral imagery. Similarly, Wang et al. (2007) had a high level of matching utilizing a neural network classification of salt marshes in the Venice Lagoon in Italy. Despite these successes, hyperspectral imagery has practical limitations because of the coarse spatial resolution and complex image processing techniques required (Hirano et al. 2003). In fact, the success of a remote sensing analysis can decrease as the landscape becomes more complex (Andrew and Ustin 2008).

As in many vegetation classification studies, our major challenges and mapping errors were associated with errors of commission. These were related to our inability to spectrally separate plant species as well as substrate subcategories (as illustrated in Fig. 5 and 6). There are apparent differences in spectral values between images and in this study we used a mosaic of many images. When we investigated areas that were incorrectly assigned following classification, it was clear that many of the errors were due to fine differences in the spectral signatures of the classes that occurred among the original images.

Rasser (2009) found that many areas with water were shallow and contained large amounts of suspended sediments, which may have impeded accurate classification of these categories. There were also several places in the image where tidal mudflats were misclassified as vegetation. This has happened in other studies as well, for example, Belluco et al. (2006) had trouble in classifying salt marsh vegetation in areas containing microphytobenthos in a salt marsh in Venice, Italy. Similarly, the reason for the misclassification in this study could be cyanobacteria mats that were observed in many tidal flats during field data collection. It is possible that these cyanobacteria were active during image acquisition, thus making it difficult for the classification methods to spectrally separate large areas of cyanobacteria mats from other vegetation.

Table 3.   **The Confusion Matrix calculated from the 2016 Imagery Classification. The overall Kappa Index was 0.70 and the overall accuracy was 75.9%. NA: not applicable**

Category	*B. frutescens*	*S. spartinae*	*B. maritima & S. virginica*	Other vegetation	Bare	Water	Total	User Accuracy %
B. frutescens	10	1	4	5	0	0	20	50.0
S. spartinae	2	26	0	3	0	0	31	83.9
B. maritima & S. virginica	0	0	42	13	11	4	70	60.0
Other vegetation	1	4	4	24	6	1	40	60.0
Bare	1	0	3	4	39	6	53	73.6
Water	1	0	0	1	0	95	97	97.9
Total	15	31	53	50	56	106	311	NA
Producer Accuracy %	66.7	83.9	79.2	48.0	69.6	89.6	NA	75.9

There was relatively little forested cover within the study area and the limited data precluded a thorough accuracy assessment. However, the classified image did appear to represent accurately forested areas in the study area as well as scattered small patches of forest (Fig.6). The integration of vegetation texture and LiDAR may have contributed to the apparent accuracy of this class.

In conclusion, the integration of high resolution multi-spectral imagery and ancillary data such as LiDAR provided a relatively accurate classification of vegetation in the Rincon Delta. Due to the increasing availability of high-resolution remote sensing data the methods developed here should prove valuable for mapping other estuarine areas. For example, the United States National Imagery Acquisition Program has begun to incorporate DMC imagery. The methods incorporated in this study are part of a growing body of research that has shown the utility of remote sensing in monitoring coastal and estuarine systems and incorporating imagery with other spatial datasets to improve classification accuracy (Goetz et al. 2008).

Landscape Vegetation Patterns in the Rincon Delta

Vegetation patterns were examined using geospatial analysis to gain a better understanding of landscape scale patterns of vegetation. These landscape patterns often confirmed some of the very obvious visual observations we have often made in the Rincon Delta. For example, one classified vegetation image shows the zonation patterns in species along tidal creeks (Fig. 14). The edges of the tidal creeks are dominated by *Borrichia frutescens*, which transition into relatively pure mixed zones of two salt tolerant succulents, *Salicornia virginica* and *Batis maritima*. The most likely explanation is the presence of the tidal creek network, which facilitates inundation and ameliorates high salinity. We also found that *B. frutescens* and *S. virginica* were most common closer to tidal creeks and the bay, and that in many areas of the

lower marsh these species dominated the overall vegetative cover. At still higher elevations, one can see patches of *Spartina spartinae*.
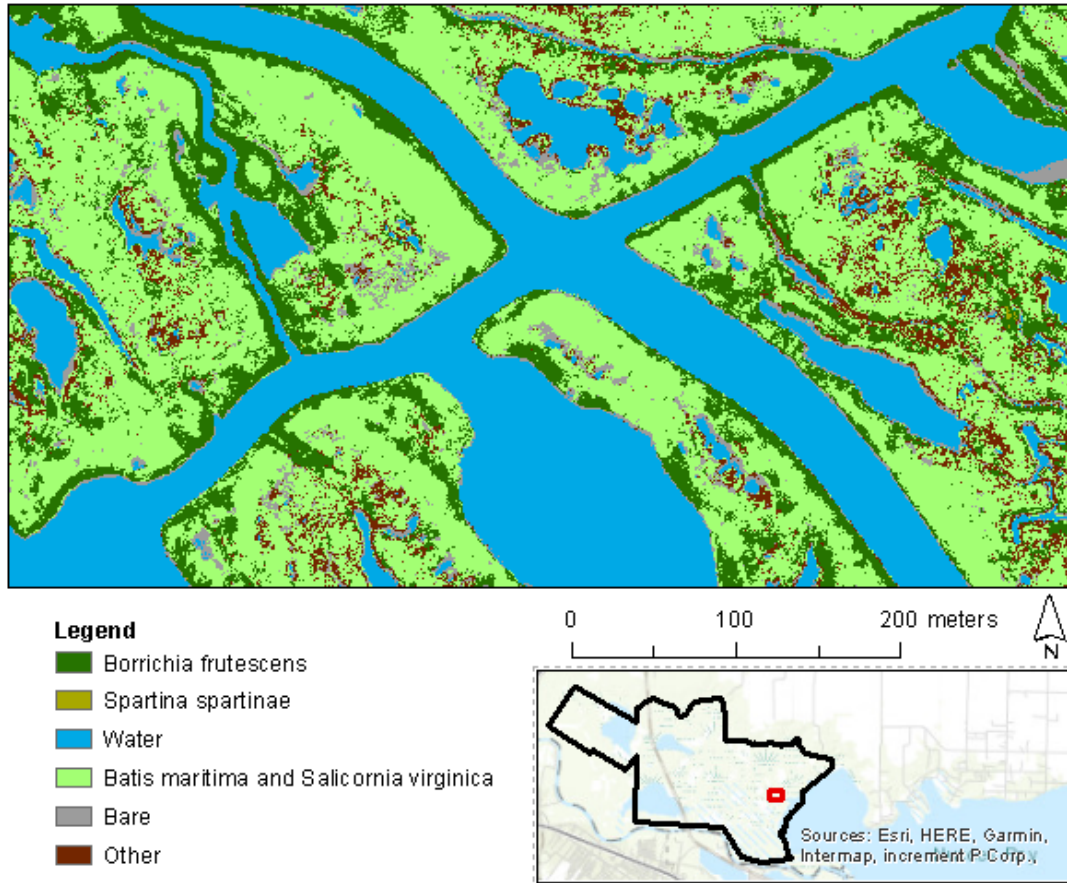
Figure 14. **The zonation of vegetation that border tidal creeks in the lower marsh is dominated by *Borrichia* at creek edges, followed by mixed and pure stands of *Batis* and *Salicornia*.**

The general six category classification of the lower Rincon Delta depicts a system that is permeated with water trapped in ponds and tidal creeks (Fig. 15). GIS analysis reveals that the open water areas compose nearly a third of the system, with unvegetated areas composing nearly another 20% (Fig. 16). This is in general agreement with Rasser (2009), who found that the vegetative cover of the lower Rincon Delta is about 50%. The most dominant plan cover type are pure stands and mixtures of *Salicornia* and *Batis*, which compose nearly 20% of the total cover. The lower levels of vegetation cover observed were similar to data available from California salt marshes. For example, remote sensing and field surveys were used to determine that non-vegetated areas accounted for between 44.6% and 86% of the ground cover at four salt marsh sites in California (Shuman and Ambrose 2003). In each of these California salt marshes *S. virginica* was the dominant plant species (13.5 to 32.8% cover). In general, *S. virginica* is the dominant plant in the lowest tidal levels of salt marshes (Li et al. 2005).

A more detailed 11-category classification shows that the contribution made by *Salicornia* and *Batis* (8% each) is about equal, confirming are own field observations (Fig. 17 and 18).
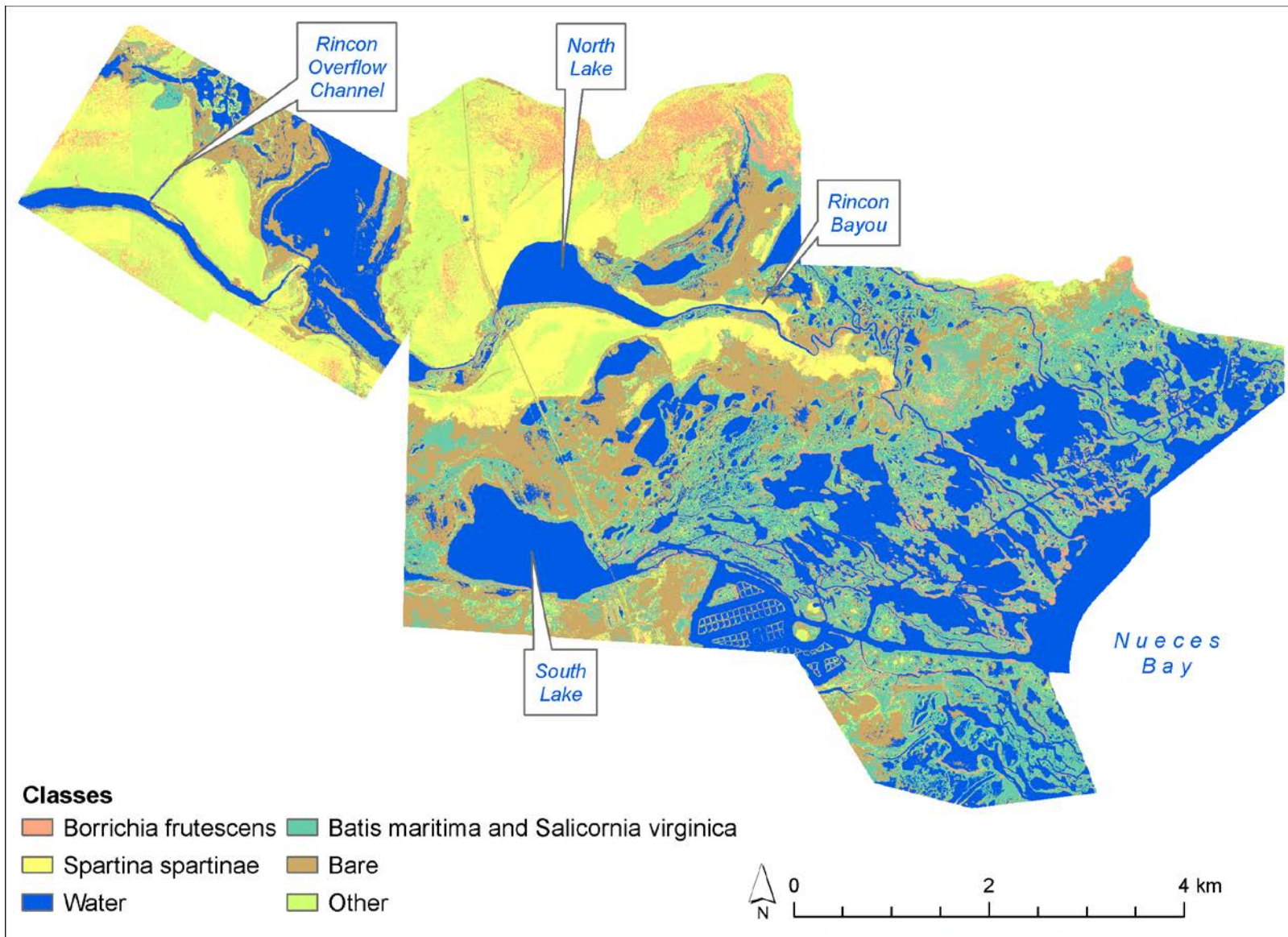
Figure 15.   **A generalized vegetation classification of the lower Rincon Delta (2016 imagery).**

As mentioned earlier, both species are succulents and highly salt tolerant and thrive in hypersaline soils. The balance of other species includes *Borrichia* (8%), *Spartina spartinae*, which is more common at higher elevations, and "other" species that include many salt tolerant perennials that are intermixed with *Borrichia, Salicornia* and *Batis*. The contribution we report for *Salicornia* is similar to that reported by Rasser (2009) in his vegetation analysis, who found that *Salicornia*'s component of the overall vegetation in the Rincon Delta was approximately 6% of the total cover (Fig. 19).

Perhaps the most conspicuous difference between the salt marsh communities of the lower Rincon Delta and many well studied North American salt marshes, particularly along the Atlantic coast, is the lack of graminoids in the lower marsh. For example, a remote sensing study of North Inlet, South Carolina found that *S. alterniflora* and *Juncus roemerianus* accounted for 83% of the estuarine area (Morris et al. 2005). *S. spartinae* is considered a brackish species with less salt tolerance than *B. frutescens* and *S. virginica*. Rasser (2009) found this species was most often found at distances greater than 113 meters from tidal creeks. A study by Sadro et al. (2007) found that *S. virginica* was inundated approximately 13% of the time. It is probable that *S. spartinae* meadows, due to their distance from tidal creeks and apparent higher elevation, are only flooded during infrequent episodes of very high-water levels such as tidal storm surges.

Percent of Total

- B. frutescens — 8%
- S. spartinae — 12%
- B. maritima & S. virginica — 18%
- Other vegetation — 14%
- Bare — 18%
- Water — 30%
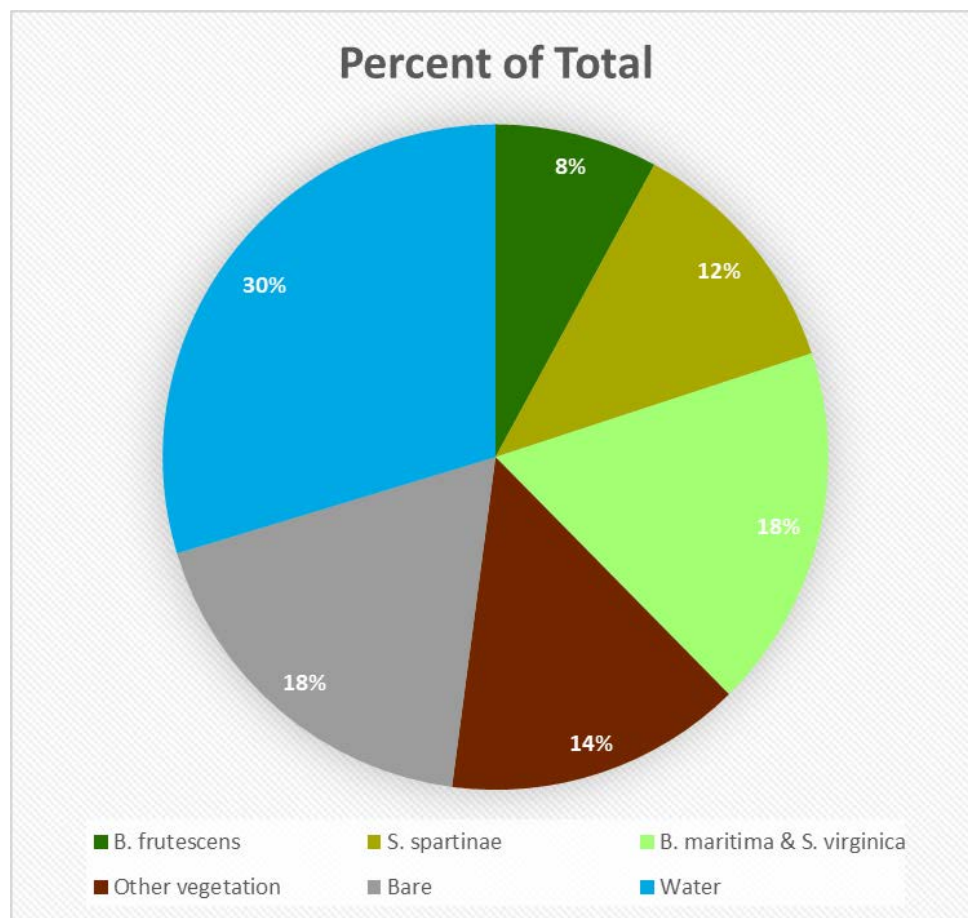
Figure 16. **The major components and contributions of the various cover types in the Rincon Delta (2016).**
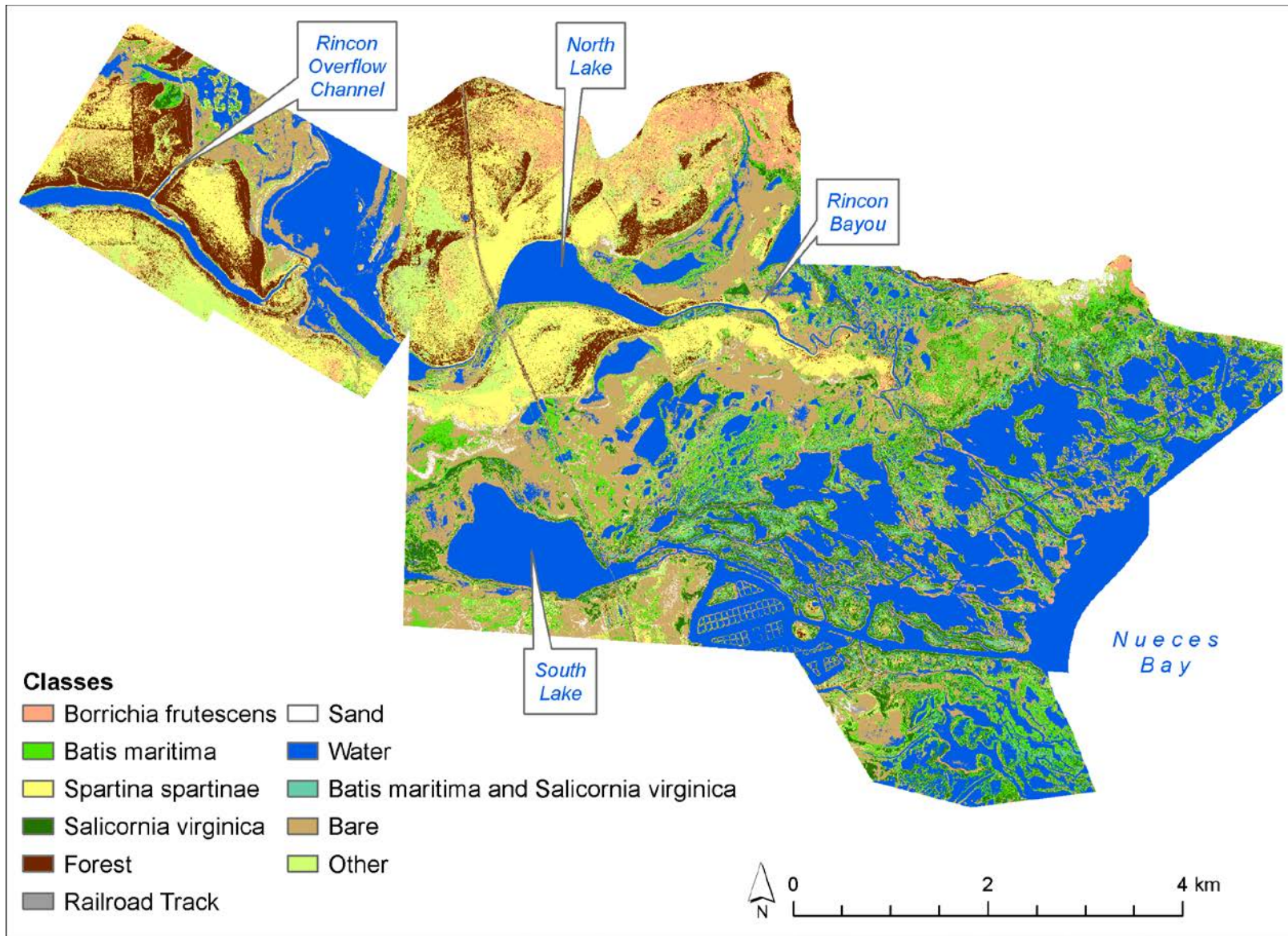
Figure 17.   **A more detailed classification of the lower Rincon Delta based on 11 category types (based on 2016 imagery).**
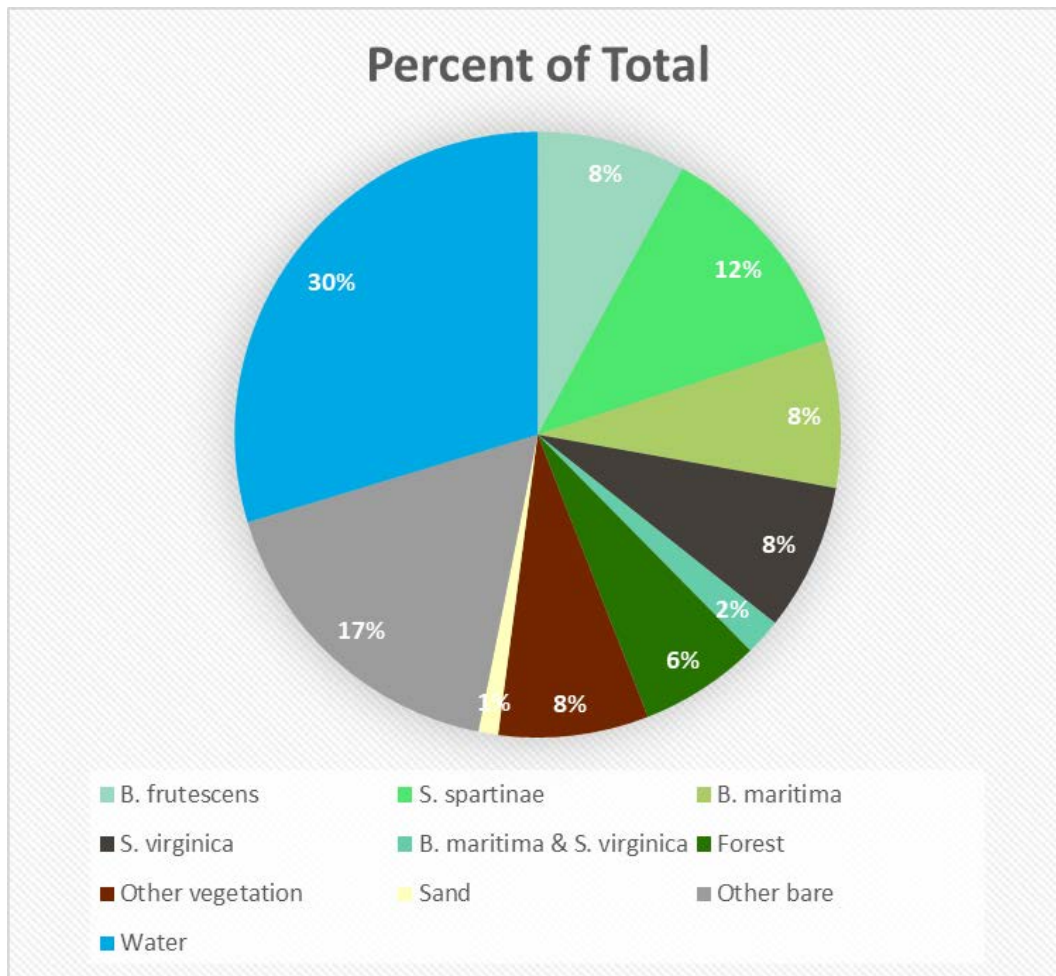
Figure 18. **The major components and contributions of eleven cover types in the Rincon Delta (based on 2016 imagery).**

S. alterniflora is only a very minor component of the Rincon Delta. Although it is found throughout the Texas coast (Kunza 2006), extensive salt marshes dominated by *S. alterniflora* are not typical. The reduced abundance of this species is probably due to the small tidal amplitude in the western Gulf of Mexico. *S. alterniflora* typically occurs within the intertidal range (Morris et al. 2005). Due to the small tidal amplitude of approximately 15 cm there is a limit amount of marsh surface that is regularly flooded, which creates ideal growing conditions for *Spartina alterniflora*.

Our results confirm the observations of Rasser (2009), who found that the abundance of *S. spartinae* increased with greater distance from the tidal creek network and Nueces Bay and increased elevation, often forming almost monospecific stands in the marsh such as the area south of North Lake (Fig. 19). This result corroborates other findings on the Gulf of Mexico coastline, where this species forms large meadows between lowland marshes and upland

communities that are relatively stable over time (Scifres et al.1980). The increase in vegetative cover of *S. spartinae* appeared to be the result of reduced tidal influence and a transition to upland plant communities. Visual inspection of the resulting classified image also shows that the largest areas of *S. spartinae* are located further from Nueces Bay.

Comparison of vegetative and non-vegetative classes between the 2009 (Rasser, 2009) and the 2016 study proved difficult, but for those categories where direct comparisons were possible, the results illustrated excellent continuity between the two studies (Table 5). Since Rasser (2009) was able obtain a significantly higher user accuracy (nearly 89%) when combining *Borrichia frutescens* and *Salicornia virginica* (and by default, *Batis maritima*), we were able to examine that assemblage against the 2016 classification. Based on the intersection of both study areas (3,445 ha), the analysis yielded only a 0.9% difference for this important group of three competing salt tolerant marsh species (Table 5). Differences between 2005 and 2016 in the remaining three classes were also low, demonstrating the inherent value of this classification approach. Improvements in image analysis software, additional training data, and a more focused effort allowed the team to improve the resolution among vegetative species in the 2016 classification. This is an exciting development and will allow a greatly expanded use of these data for modeling and assessment.

Table 4.   **Vegetative communities in the Rincon Delta based on the 2016 classification (3817 hectares).**

Cover Class	Area (ha)	Percent of Total Area
Borrichia frutescens	302	7.9
Batis maritima	300	7.9
Spartina spartinae	459	12.0
Salicornia virginica	300	7.9
Batis maritima and *Salicornia virginica*	74	1.9
Forest	246	6.5
Other vegetated	306	8.0
Railroad track	13	0.4
Sand	40	1.1
Bare (other than sand and railroad track)	642	16.8
Water	1133	29.7
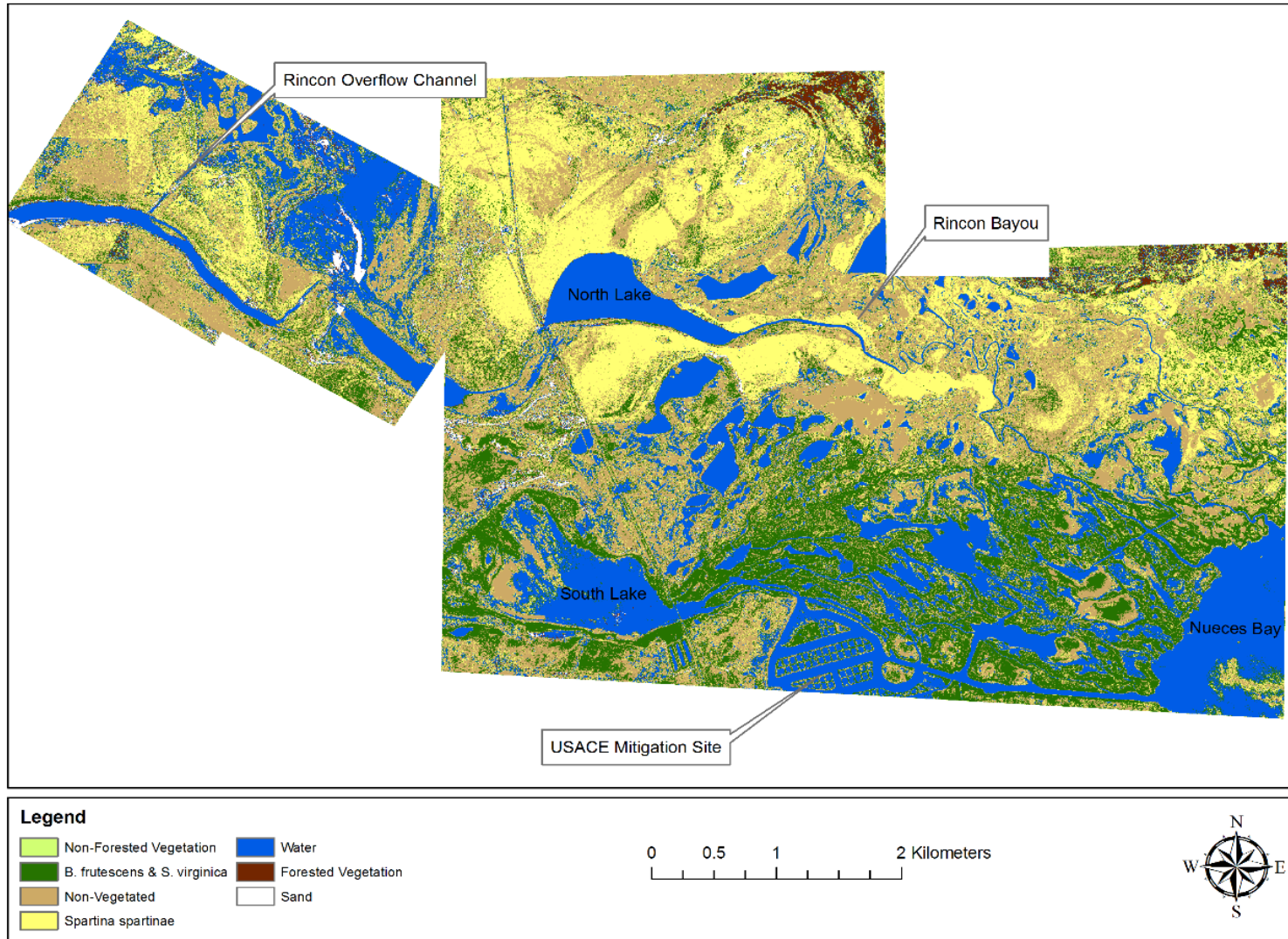
Figure 19. **Classified image of study area based on classification of digital aerial imagery acquired 1 November 2005 (from Rasser, 2005).**

Table 5.   **Comparison of the vegetative communities in the Rincon Delta based on the direct intersection of the 2005 (Rasser 2009) and 2016 classification area (3445 hectares).**

Cover Class	Percent of Total Area	
	2005	2017
Borrichia frutescens, Salicornia virginica, Batis maritima	23	23.9
Spartina spartinae	17.7	13.3
Water	26.1	28.4
Sand	2.6	1.1

Long-Term Vegetation Response to Drought and Salinity

Previous studies have shown that the emergent plant community is responsive to variations in salinity and freshwater inflow (U.S. Bureau of Reclamation 2000; Alexander and Dunton 2002; Forbes and Dunton 2006). Patterns in species composition observed over nearly two decades at three sites in the Rincon Delta (Fig. 20) reveal distinct vegetation responses to drought. This dataset is unique in that it considers both some of the wettest (2002 -2004) and the driest periods (2009-2011) since reservoir construction. Plant communities observed during early droughts (1999-2001) were present during subsequent dry periods in 2005 and 2008. These drought period communities were characterized by a high abundance of *S. virginica* and a low abundance of *S. alterniflora*. The time required for the reappearance of drought period assemblages was related to the magnitude of freshwater inflow events during the preceding wet period. High freshwater inflows during 2002-2004, extended the time period between the reemergence of drought period vegetation communities. The sensitivity to drought periods is best reflected by variations in pore water salinity, which can increase to values exceeding 100 (Fig. 21). The cover of *Borrichia frutescens* declined dramatically in 2009 when pore water salinities were consistently above 45. *Borrichia* cover has been slow to recover over the past decade, reaching values that approach its cover before the 2009 drought began (Fig. 21).

Texas Water Development Board Report Contract #1600011971
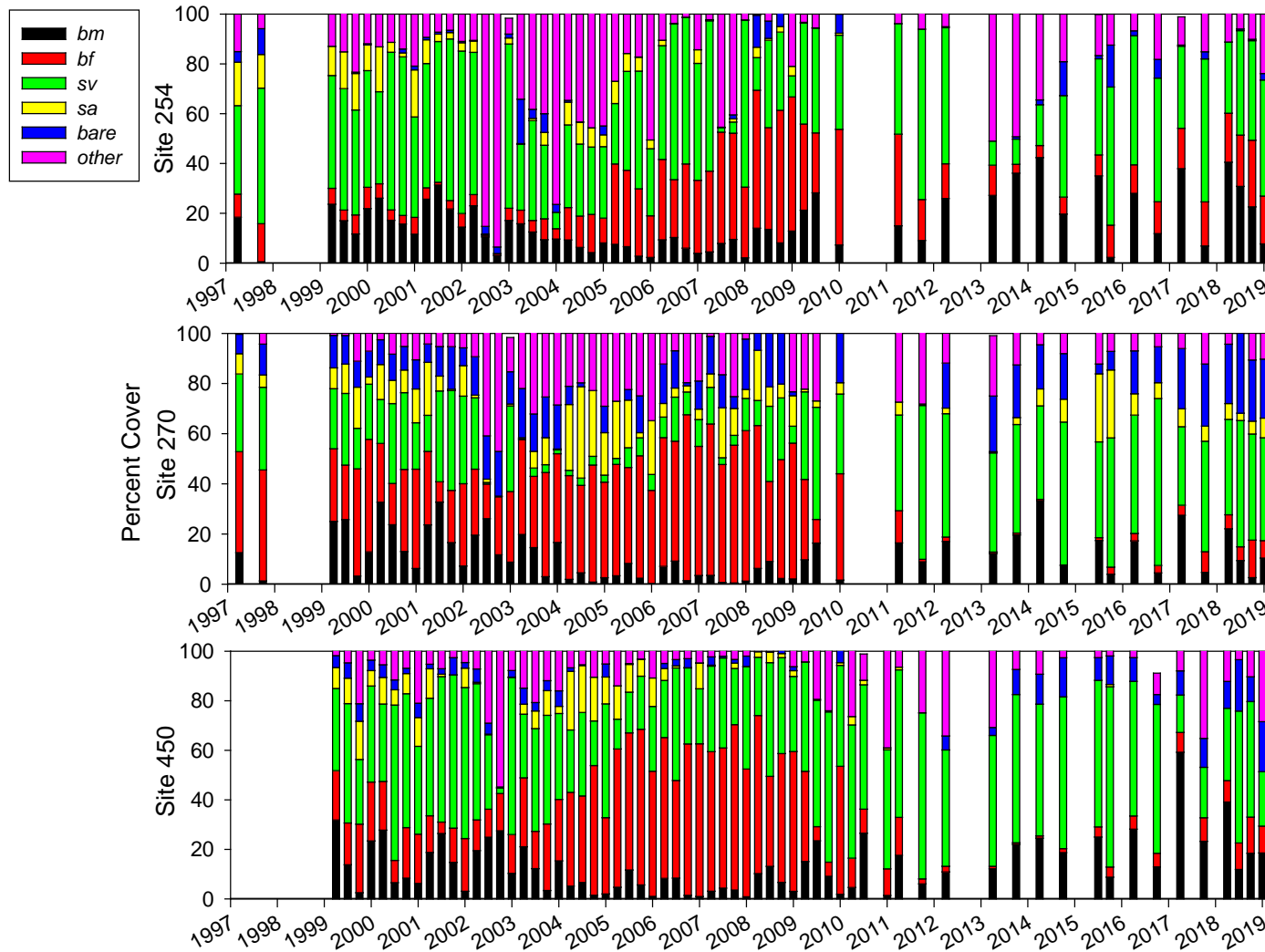
Figure 20. Quarterly percent cover of emergent plants at selected sites in the Nueces River Delta for the period 1999-2019.

Texas Water Development Board Report Contract #1600011971
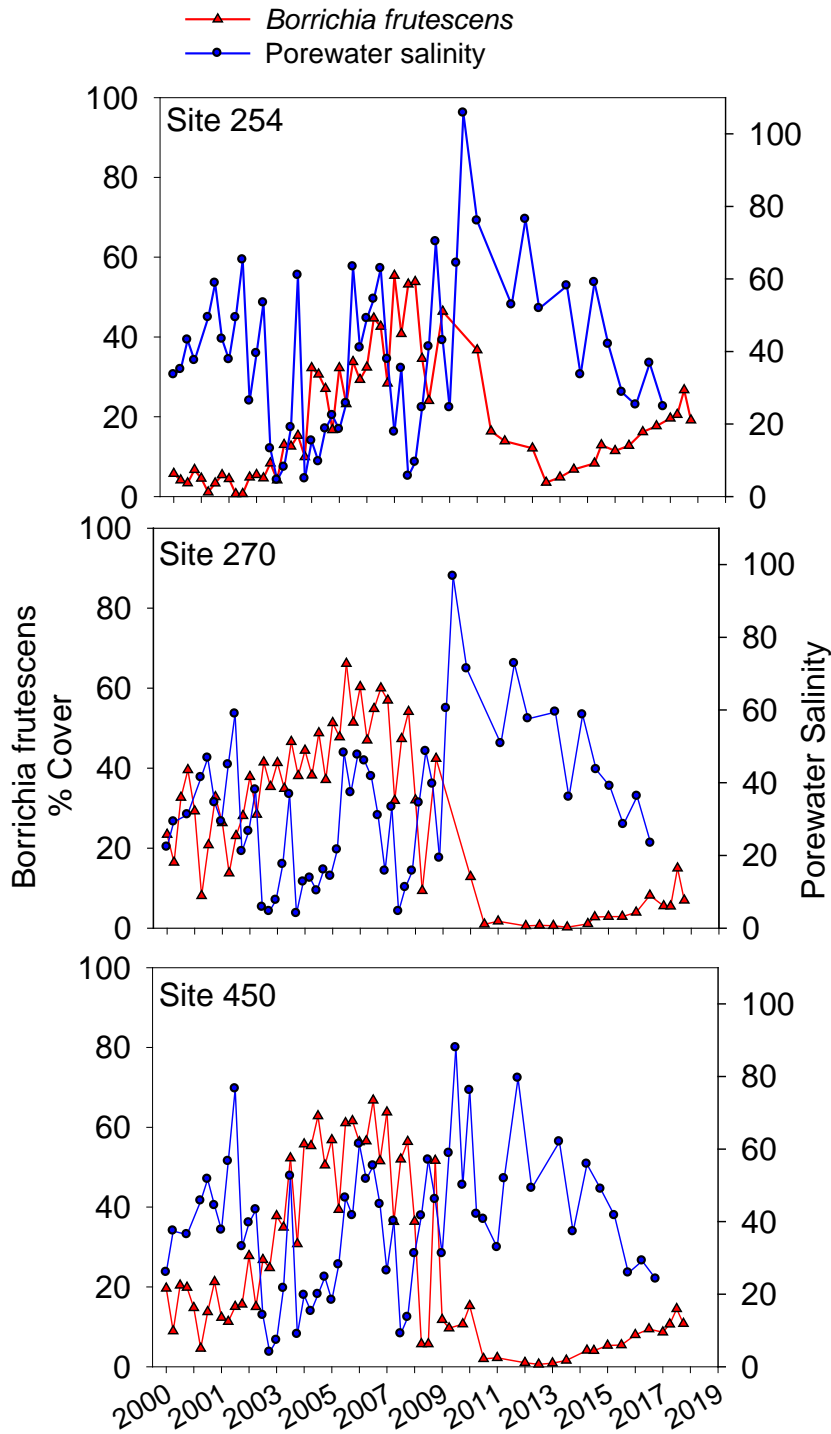
Figure 21. Porewater salinity (blue circles) and percent cover of *Borrichia frutescens* (red triangles) along the creek bank in the low marsh. Porewater salinities exceeding about 45 result in declines of *B. frutescens* abundance.

Estimation of Rate of Shoreline Erosion

Rasser and Dunton (2007) examined color infrared photographs acquired on 26 September 1997 and 1 November 2005 to estimate rates of shoreline erosion of the Nueces River Delta. They measured the distance between the 1997 and 2005 shorelines to estimate the average erosion along the length of the study area based on the selection of random points (Fig 22). Based on the distance between the 1997 and 2005 shorelines at each of the 30 locations along the average shoreline retreat was 20.15 m (n=30, sd = 7.4 m) for the period 1997 – 2005 or 2.5 m year^{-1} for a net loss of 4.1 ha within the defined study area (Rasser and Dunton, 2007).

Our comparison of 2005 and 2016 imagery show an even greater annual rate of shoreline loss (Fig. 23). Based on our preliminary measurements, we estimate that shoreline erosion could be occurring as fast as 4.5 m yr^{-1}. More importantly, comparison of the 2005 and 2016 imagery show breaching of Nueces Bay into large ponds of the lower delta. This breaching serves to further accelerate marsh loss and seriously compromises estuarine habitat of the lower marsh system. Factors contributing to the continued erosion of the Delta shoreline are reduced sediment delivery owing to the dam construction on the Nueces River and a relative sea level rise, which at 6 mm yr^{-1} in the Coastal Bend is about twice that of the global average.

The lower marsh assemblage of *B. frutescens* and *S. virginica* appears to be most impacted by erosion as these species grow close to tidal creeks and Nueces Bay. An estimated 80% of the area lost to erosion consists of this vegetation class (Rasser, 2009). It is difficult to estimate the total area lost to erosional processes because our imagery only covers a portion of the entire Rincon Delta shoreline that is in contact with Nueces Bay. However, the erosion of the Delta has clearly resulted in large losses of wetlands dominated by *B. frutescens* and *S. virginica.*

Concluding Statements

The decadal assessments of areas occupied by water, sand, and vegetation is critical to understanding how the Rincon Delta is responding to regional climate, sea level rise, and freshwater inflow events. The vegetation is particularly sensitive to climatic conditions and reflects long-term changes in the hydrological regime. The patterns apparent in the imagery are also reflective of salinity, which is a product of droughts and/or reduced freshwater inflow events.

Our results suggest that if droughts become longer and more frequent, species replacements are likely to occur. Rasser (2009) hypothesized that under increasing saline conditions, *S. virginica* will likely replace *S. alterniflora* and make up even a greater proportion of the overall community. Drought conditions may also decrease the overall extent of emergent salt marsh plants in the Rincon Delta as decreases in freshwater inflow, concurrent with more erratic and possibly decreasing precipitation (Forbes and Dunton 2006).

One way in which environmental stress is expressed in the vegetation community is through zonation. Zonation is characterized by distinct banding or spatial separation of species depending on differing tolerance to environmental stress and interspecific competition for resources (Adams 1963; Pennings et al. 2005). Typically, this occurs in response to variations in inundation frequency corresponding with an elevation gradient (Rasser 2009).

Texas Water Development Board Report Contract #1600011971
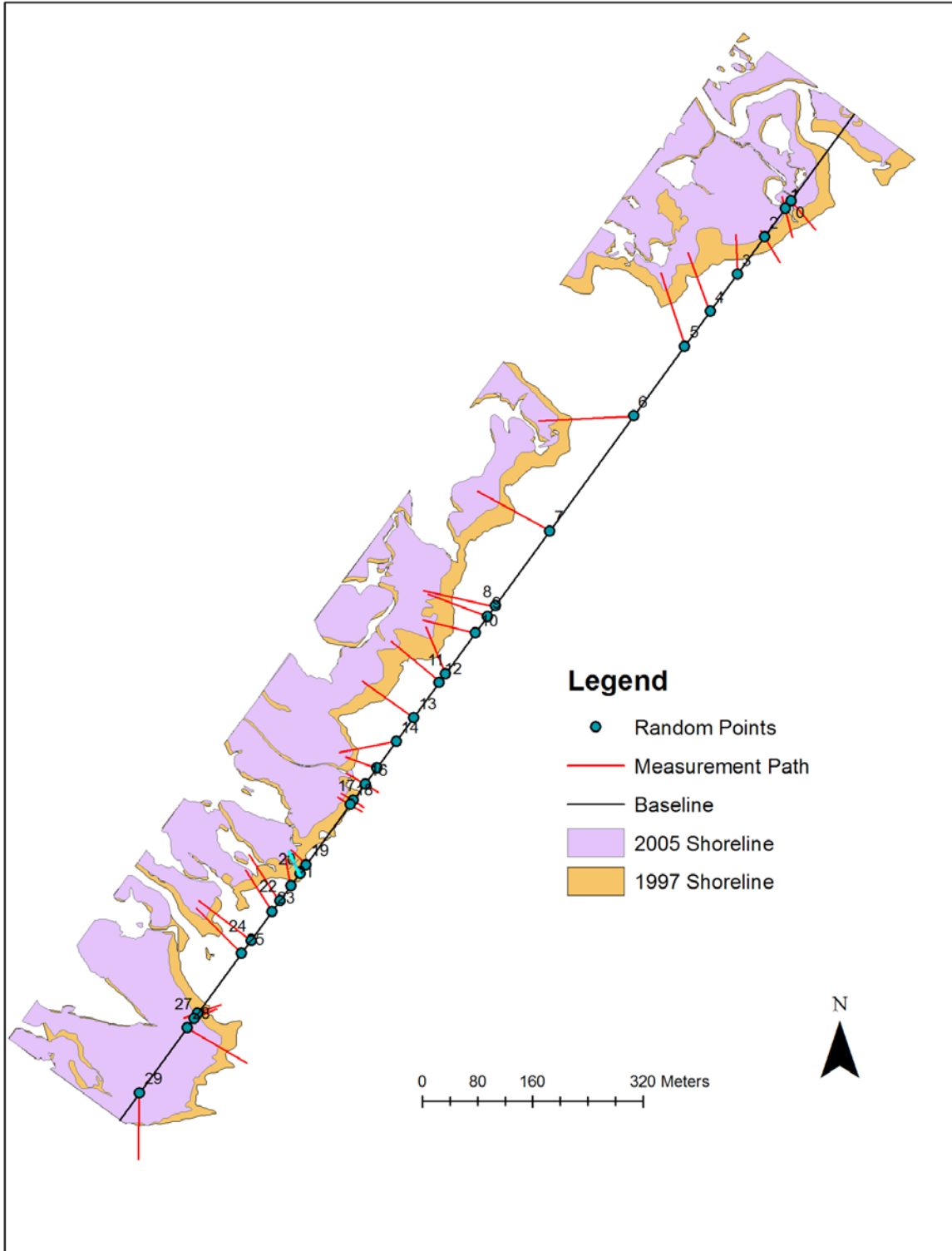
Figure 22. Shoreline erosion was measured at 30 random points along the study area baseline. The distance between the 1997 and 2005 shorelines was determined from each point perpendicular to the shoreline along the measurement path.
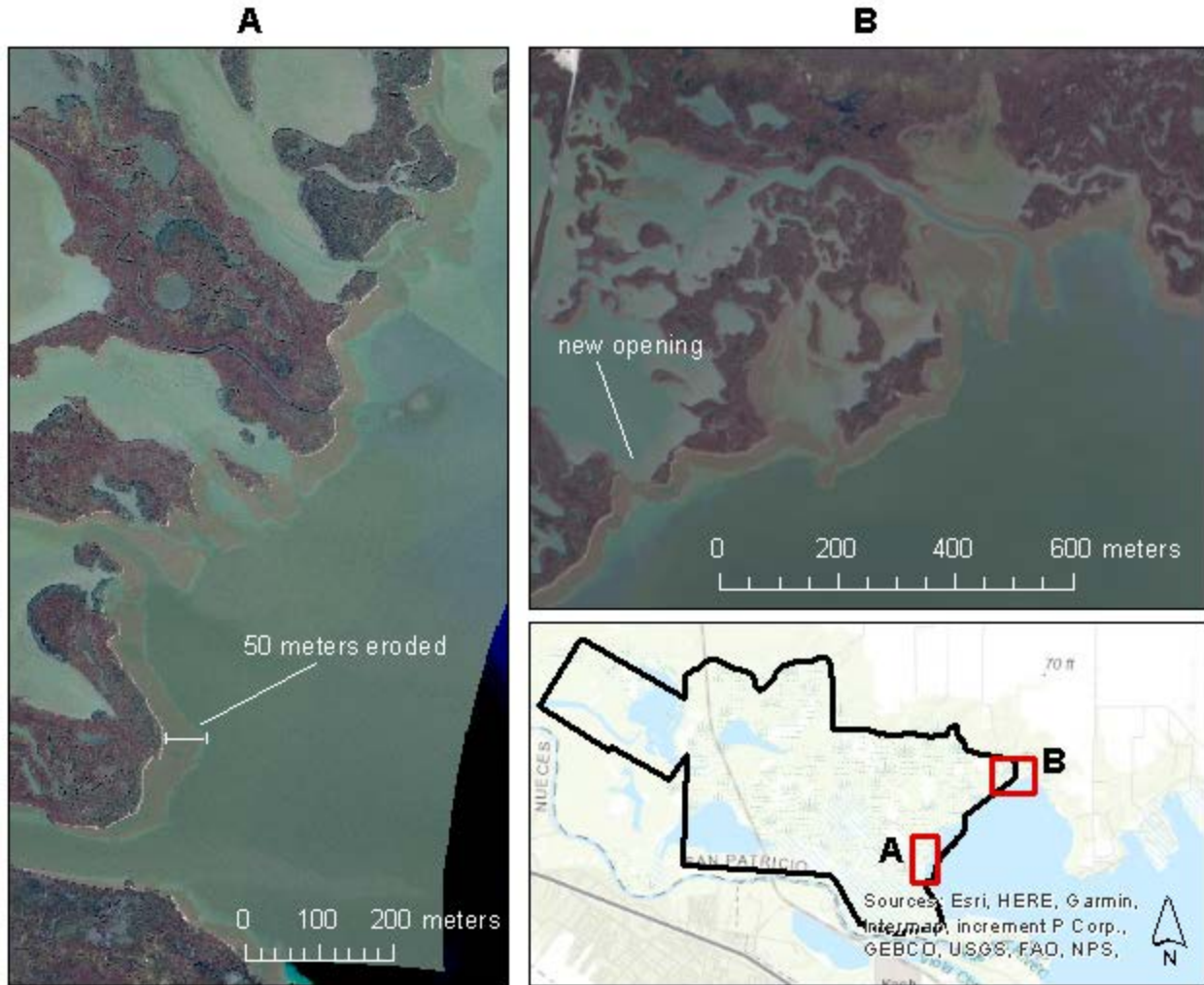
Figure 23. **A comparison of the 2005 and 2016 imagery reveals shoreline erosional losses up 4.5 m yr^{-1} and significant breaching events of the Rincon Delta.**

Zonation can be observed in the Nueces Delta under intermediate flooding disturbance. However, during extreme drought or flooding, zonation bands are dissolved, and extensive bare areas are created (Alexander and Dunton 2002). Large magnitude events, such as floods, are known to cause wholesale reorganization of the vegetation community (Forbes and Dunton 2006).

This finding is important because the use of emergent vegetation as indicators of ecosystem condition is predicated on the assumption that community structure is predictable under a given set of hydroclimatic conditions. We have found that vegetation communities in the Rincon Bayou Delta follow a predictable trajectory. First, bare areas, which are created following large inflow events, are initially colonized by stress intolerant species such as *S. alterniflora* and *Suaeda maritima*. In the absence of freshwater inundation, these individuals are eventually replaced by the moderately stress tolerant *B. frutescens* (Fig. 21). Finally, with the onset of

drought conditions, we see the replacement of nearly all species by the stress tolerant *S. virginica* (Forbes and Dunton 2006). Interestingly, following freshwater inflow events, the opposite occurs, and we see the displacement *S. virginica* by *B. frutescens* (Forbes and Dunton 2006). In addition, a variety of studies determined that *S. virginica* is resilient to extreme environmental stress (Zedler 1983; Rasser 2009). Clearly, frequent freshwater inflow events are required for the maintenance of an estuarine *S. alterniflora* creekbank habitat, which although present in the Rincon Delta, is very limited in its extent.

The ongoing patterns of displacement, invasion, and re-establishment of plant species in response to alternating periods of drought with periods of precipitation are well reflected in vegetative species composition (Fig. 20). At site 270, the increases and decreases in percent cover in *S. alterniflora* are coincident with corresponding decreases and increases in the cover of *S. virginica.* The overall community response is sufficient to produce clusters of vegetation communities that correspond to dry and wet periods using a multidimensional scaling ordination (Stachelek and Dunton, 2013). These analyses clearly show that plant communities undergo major quantifiable changes in response to precipitation. However, based on the patterns in vegetative cover (Fig. 20) and the comparison of major plant assemblages between 2005 and 2016 (Table 5), long-term shifts in vegetative patterns are not evident in our data that indicate a clear trajectory of ecosystem change. Certainly, variations in vegetation assemblages occurred during the 11-yr period from 2005 to 2016 (Fig. 20), but the resiliency of the vegetation to large swings in salinity has not created additional bare areas that are unsuitable for plant establishment.

Acknowledgments

References

Adam. P. 1990. Salt Marsh Ecology. Cambridge University Press, Melbourne.

Adams, D.A. 1963. Factors influencing vascular plant zonation in North Carolina salt marshes. Ecology 44:445-456.

Alexander, H.D. and K. H. Dunton. 2002. Freshwater inundation effects on emergent vegetation of a hypersaline salt marsh. Estuaries and Coast, 25:1559-2731.

Alexander, H.D. and K. H. Dunton. 2006. Wastewater effluent as an alternative freshwater source in a hypersaline salt marsh: Impacts on salinity, inorganic nitrogen, and emergent vegetation. Journal of Coastal Research, 22:377 - 392.

Armstrong, N.E. 1987. The ecology of open-bay bottoms of Texas: a community profile. U.S. Fish and Wildlife Service Biological Report. 85:7.12. 104 pages.

Andrew, M.E. and S.L. Ustin. 2008. The role of environmental context in mapping invasive plants with hyperspectral image data. Remote Sensing of Environment, 112:4301-4317.

Belluco, E., M. Camuffo, S. Ferrari, L. Modenese, S. Silvestri, A. Marani and M. Marani. 2006. Mapping salt-marsh vegetation by multispectral and hyperspectral remote sensing. Remote Sensing of Environment, 1:54-67.

Chapman V.J. 1940. Succession on the New England Salt Marshes. Ecology, 21:279-282.

Chen, K., C. Jacobson and R. Blong. 2001. Using NDVI image texture analysis for bush-fire prone landscape assessment. Paper presented at the 22nd Asian Conference on Remote Sensing. November 5-9 2001, Singapore.

Chen, R.G., Fedosejevs, M. Tisacareno-Lopez and J.G. Temple. 2006. Assessment of MODIS-EVI and VEGETATION-NDVI composite data using Agricultural measurements: An example of corn field in western Mexico. Environmental Monitoring and Assessment, 119:69-82.

Dunton, K.H., B. Hardgree and T.E. Whitledge. 2001. Response of estuarine marsh Vegetation to interannual variations in precipitation. Estuaries, 24:851-861.

Eastwood, J.A., M.G. Yates, A.G. Thomson and R.M. Fuller. 1997. The reliability of vegetation indices for monitoring salt marsh vegetation cover. International Journal of Remote Sensing, 18: 3901-3907.

Ehlers, M.M., Gaehler and R. Janowsky. 2006. Automated techniques for environmental monitoring and change analysis for ultra high resolution remote sensing data. Photogrammetric Engineering and Remote Sensing, 72:835-844.

Forbes, M.G. and K.H. Dunton. 2006. Response of a subtropical estuarine marsh to local climate change in the southwestern Gulf of Mexico. Estuaries and Coasts, 29:1242-1254.

Gilmore, M.S., E.H. Wilson, N. Barrett, D.L. Civco, S. Prisloe, J.D. Hurd and C. Chadwick. 2008. Integrating multi-temporal spectral and structural information to map wetland vegetation in a lower Connecticut River tidal marsh. 2008. Remote Sensing of Environment, 112:4048-4060.

Goetz, S.J., N. Gardiner and J.H. Viers. 2008. Monitoring freshwater, estuarine and near-shore benthic ecosystems with multi-sensor remote sensing: An introduction to the special issue,112:3993-3995.

Henley, D.E. and D. G. Rauschuber. 1981. Freshwater needs of fish and wildlife resources in the Nueces-Corpus Christi Bay Area, Texas: a literature synthesis. U.S. Fish and Wildlife Service, Office of Biological Services. Washington. D.C. FWS/OBS-80/10.410 pages.

Hirano, A., M. Madden and R. Welch. 2003. Hyperspectral image data for mapping wetland vegetation, Wetlands 23:436-448.

Higinbothom, C.B., M. Alber and A.G. Chalmers. 2004. Analysis of tidal marsh vegetation patterns in two Georgia estuaries using aerial photography and GIS. Estuaries, 27:670-683.

Huete, A.R. 1988. A soil adjusted vegetation index. Remote Sensing of Environment, 25:295-309.

Kent, B. and Mast, J.N., 2005. Landscape change analysis of San Dieguito Lagoon, California: 1928-1994. Wetlands, 25: 780-787.

Kunza, A.E. 2006. Patterns of plant diversity in two salt marsh regions. Master of Science Thesis, University of Houston, Houston, Texas. 70 pages

Laba, M., R. Downs, S. Smith, S. Welsh, C. Neider, S. White, M. Richmond, W. Philpot and P. Baveye. 2008. Mapping invasive wetland plants in the Hudson River National Estuarine Research Reserve using quickbird satellite imagery. Remote Sensing of Environment, 112: 286-300.

Landis, J.R. and G. Koch 1997. The measurement of observer agreement for categorical data. Biometrics, 33:159-174.

Lathrop, R.G., P. Montesano and S. Hang. 2006. A multi-scale segmentation approach to mapping seagrass habitats using airborne digital camera imagery. Photogrammetric Engineering and Remote Sensing, 72:665-675.

Lefskey, M.A., Warren, B.C., G.G. Parker, and D.J. Harding. 2002. LiDAR remote sensing for ecosystem studies. Bioscience, 52:19-30.

Li, L., S.L. Ustin and M. Lay. 2005. Application of multiple endmember spectral mixture analysis (MESMA) to AVIRIS imagery for coastal salt marsh mapping: a case study in China Camp, CA, USA. International Journal of Remote Sensing 26:5193-5207.

Lillesand T., and R.W. Kiefer. 2004. Remote Sensing and Image Interpretation. John Wiley & Sons Hoboken, NJ, 724 pages.

McCoy, R.M. 2005. Field Methods in Remote Sensing. The Guilford Press. New York.

Morris, J.T., D. Porter, M. Neet, P.A. Noble, L. Schmidt, L. A. Lapine and J. R. Jensen. 2005. Integrating LIDAR elevation data, multi-spectral imagery and neural network modeling for marsh characterization. International Journal of Remote Sensing, 26:5221-5234.

Murphy, R.J., T.J. Tolhurst, M.G. Chapman and A.J. Underwood. 2004. Estimation of surface chlorophyll on exposed mudflat using digital colour-infrared (CIR) photography. Estuarine, Coastal and Shelf Science, 59:625-638.

Pengra, B.W., C.A. Johnston and T.R. Loveland. 2007. Remote Sensing of Environment, 108: 74-81.

Pennings, S.C. and M.D. Bertness. 2001. Salt marsh communities. Marine Community Ecology (eds M.D. Bertness, S.D. Gaines, and M.E. Hay). pp. 289-316. Sinaeur Associates, Sunderland Massachusetts.

Pennings, S.C., M. Grant and M.D. Bertness. 2005. Plant zonation in a low-latitude salt marsh: disentangling the roles of flooding, salinity, and competition. Journal of Ecology, 93:159-167.

Pritchard, D. W. 1967. What is an estuary, physical viewpoint. In: G. H. Lauf (editor): *Estuaries.* American Association for the Advancement of Science, Washington D.C., publ. no. 83.

Provost, S., M. Van Til, B. Deronde and A. Knotters. 2005. Remote sensing of coastal vegetation in the Netherlands and Belgium Pages 139-149 in Proceedings "Dunes and Estuaries 2005". International Conference on Nature Restoration Practices in European Coastal Habitats, Koksijde, Belgium, September 19-23, 3005. Herrier, J, -L, J. Mees, A. Salman, J. Seys, H. Van Nieuwenhuyse and I. Dobbrlaere Eds. VLIZ Special Publication 19, xiv 685 pages.

Qi, J., A. Chehbouni, A.R. Huete, Y.H. Kerr and S. Sorooshian. 1994. A modified soil adjusted vegetation index. Remote Sensing of Environment 48:119-126.

Rasser, M.K. 2009. The Role of Biotic and Abiotic Processes in the Zonation of Salt Marsh Plants in the Nueces River Delta, Texas. Ph.D. Dissertation. The University of Texas at Austin. 166 p.

Rasser, M.K. and K.H. Dunton. 2007. Analysis of coastal erosion of the Nueces Delta shoreline. Project Report for Coastal Bend Bay and Estuaries Program. 8 p.

Roy, P.S. 1984. New South Wales estuaries: their origin and evolution. Pages 99-121. In Coastal Geomorphology in Australia, editor B. G. Thom. Academic Press, Sydney, AU.

Sadro, S., M. Gastil-Buhl and J. Melack. 2007. Characterizing patterns of plant distribution in a southern California salt marsh using remotely sensed topographic and hyperspectral data and local tidal fluctuations. Remote Sensing of Environment, 110: 226-239.

Sanderson, E.W., S. L. Ustin and T. C. Foin. 2000. The influence of tidal channels on the distribution of salt marsh plant species in Petaluma Marsh, CA, USA. Plant Ecology, 146:1385-29-41.

Scifres, C.J., J.W. McAtee and D.L. Drawe. 1980. Botanical, edaphic, and water relationships of gulf cordgrass (Spartinae spartinae [Trin.] Hitchc.) and associated communities. The Southwestern Naturalist, 25:397-410.

Silvestri, S., N. Marani and A. Marani. 2003. Hyperspectral remote sensing of salt marsh vegetation morphology and soil topography. Physics and Chemistry of the Earth, 28:15-25.

Shuman, C.S. and R. F. Ambrose. 2003. A comparison of remote sensing and ground based methods for monitoring wetlands restoration success. Restoration Ecology, 11:325-333.

Stachelek, J. and K.H. Dunton. 2013. Freshwater inflow requirements for the Nueces Delta, Texas: Spartina alterniflora as an indicator of ecosystem condition. Texas Water Journal 4(2): 62-73.

Tucker, C.J. 1979. Red and photographic infrared linear combinations for monitoring vegetation. Remote Sensing of Environment, 8:127-150.

U.S. Bureau of Reclamation. 2000. R. G. Harris (ed.). Concluding Report: Rincon Bayou Demonstration Project. Volume II. Findings. U.S. Department of the Interior. Bureau of Reclamation, Austin, Texas, USA.

Valta-Hulkkonen, K., P. Pellikka, H. Tankskanen, A. Ustinov and O. Sandman. 2009. Digital false color aerial photographs for discrimination of aquatic macrophyte species. Aquatic Botany, 75:71-88.

Verrelst, J., G.W. Geerling, K.V. Sykora and J.G.P.W. Clevers. 2008. Mapping of aggregated floodplain plant communities using image fusion of CASI and LIDAR data. International Journal of Applied Earth Observation and Geoinformation, 11: 83-94.

Wang, C., M. Menenti, M. Stoll, E. Belluco and M. Marani. 2007. Mapping mixed vegetation communities in salt marshes using airborne spectral data. Remote Sensing and Environment, 107:559-570.

Ward, G.H. 1985. Evaluation of marsh enhancement by freshwater diversion. Journal of Water Resources Planning and Management, ASCE 111:1–23.

Wulder, M.A., R.J. Hall, N. Coops and S.E. Franklin. 2004. High spatial resolution remotely sensed data for ecosystem characterization. Bioscience 54:511-521.

Zedler, J.B., J.C. Callaway, J.S. Desmond, G. Vivian-Smith, G.D. Williams, G. Sullivan, A.E. Brewster and B.K. Bradshaw. 1999. California salt-marsh vegetation: An improved model of spatial pattern, Ecosystems. 2:19-35.